Supporting Information

Superatomic interconversion causes reversible on-off luminescence of doped silver nanoclusters

Wenjie Lei,[†a] Yang Shao,[†b] Fangya Ren,[†a] Mengdi Guo,[d] Qing You,[e] Xianjun Fang,[f] Jie Kong[b], Meng Zhou*[b], Baoqi Yin*[a] and Zhixun Luo[c]*

[a]School of Pharmacy, Anhui University of Chinese Medicine, Hefei, 230012, Anhui, P. R. China

[b]Hefei National Laboratory for Physical Sciences at the Microscale, University of Science and Technology of China, Hefei, Anhui 230026, China

[c]Beijing National Laboratory for Molecular Sciences (BNLMS), State Key Laboratory for Structural Chemistry of Unstable and Stable Species, Institute of Chemistry, Chinese Academy of Sciences, Beijing 100190, P. R. China

[d]Hubei Key Laboratory of Energy Storage and Power Battery, School of New Energy, Hubei University of Automotive Technology, Shiyan, Hubei 442002 P. R. China
E-mail: mdguo@huat.edu.cn

[e]Institute of Solid State Physics, Hefei Institutes of Physical Science (HFIPS), Chinese Academy of Sciences, Hefei 230031, P. R. China

[f]School of Pharmacy, Anhui Medical University, Hefei, 230032, China

† These authors contributed equally to this work.

∗ Corresponding author.

E-mail address: mdguo@huat.edu.cn; mzhou88@ustc.edu.cn; yinbaoqi@ahtcm.edu.cn;

Experimental Reagents

Potassium tetrachloroplatinate (II) ($H_2PtCl_6 \cdot 6H_2O$, 99%), Palladium (II) diacetate ($Pd(CH_3COO)_2$, 99%), Silver trifluoromethanesulfonate (AgOTf), Sodium borohydride ($NaBH_4$), 1,3-bis(diphenyphosphino)propane (DPPP, 98%), Sodium hexafluoroantimonate ($NaSbF_6$, >99%) was purchased from Bide Pharmatech Ltd. (Shanghai, China). Solvents, including dichloromethane (DCM, A.R.), trichloromethane (TCM, A.R.), Tetrahydrofuran (THF, A.R.)diethyl ether (Et_2O, A.R.), methanol (MeOH, A.R.), Ethanol (EtOH, A.R.) acetonitrile (CH_3CN or ACN, A.R.), N, N-dimethylformamide (DMF, A.R.), dimethylsulfoxide (DMSO, A.R.), tetrahydrofuran (THF, A.R.), acetone (C_3H_6O, A.R.) and n-hexane/pentane (*n*-Hex/Pent, A.R.) were purchased from Sinopharm Chemical Reagent Co. Ltd. (Shanghai, China). The water used in all experiments was ultrapure (resistivity 18.2 MΩ·cm), produced by a Milli-Q NANO pure water system. All reagents were purchased commercially and used without further purification.

Characterizations

The single-crystal X-ray diffraction (SC-XRD) data were collected on a Bruker D8 VENTURE AXS photon 100 diffractometer with Helios mx multilayer monochromator using Ga-Kα (λ = 1.34139 Å) radiation for M_1Ag_{18} (M= Pd, Pt). Cambridge Crystallographic Data Center (CCDC) depository number of Pd_1Ag_{18} and Pd_1Ag_{18} are 2476700 and 2476701, respectively. Electrospray ionization (ESI) mass spectra were recorded on a Waters Q-TOF mass spectrometer using a Z-spray source. And the samples were dissolved in CH_2Cl_2 solvent (~0.5 g/L) and injected into the chamber at 5 μL/min. All UV-Vis adsorption spectra were acquired using a UV-8000 spectrophotometer (METASH, China). X-ray photoelectron spectroscopy (XPS) measurements were performed with an ESCALAB 250 Xi XPS system supplied by Thermo Scientific. The photoluminescence properties of the nanoclusters in DMF were

recorded by a FL-8500 fluorescence spectrophotometer (Perkinelmer, America) using a xenon lamp as the excitation source and the excitation wavelength was set at 420nm. Absolute PL quantum yields (PLQYs) were measured with dilute solutions of nanoclusters on FLS1000 spectrometer from Edinburgh Instruments Ltd.

TA Testing.

Femtosecond transient absorption (fs-TA) measurements were carried out using a home-built pump–probe setup. The fundamental laser pulse (800 nm, 35 fs pulse width, 1 kHz repetition rate) was generated by a regeneratively amplified Ti:sapphire laser (Coherent Astrella-Tunable-USP, USA). The output beam was divided into pump and probe arms by a broadband beamsplitter. A commercially available collinear optical parametric amplifier (Light Conversion) was used to generate a tunable pump pulse. The probe beam passed through a computer-controlled optical delay line and was then focused onto a thin sapphire plate to generate a white-light supercontinuum. This continuum was split by a broadband 50/50 beamsplitter into signal and reference beams covering the spectral range of 440–790 nm. The focused pump and probe pulses were spatially overlapped inside a sample cell (1 mm quartz cuvette). A half-wave plate inserted into the pump beam path was used to set the mutual polarization between pump and probe pulses to the magic angle (54.7°), enabling the measurement of isotropic transient signals. Nanosecond transient absorption (ns-TA) spectra were recorded using a commercial spectrometer (Time-Tech Spectra). The pump source for the ns-TA measurements was identical to that used in the fs-TA experiments. The ns-TA probe beam was generated by a supercontinuum laser (LEUKOS-DISCO, France) operating at a repetition rate of 2 kHz, delivering pulses with a width of 700 ps to 1 ns over a spectral range of 410–950 nm.

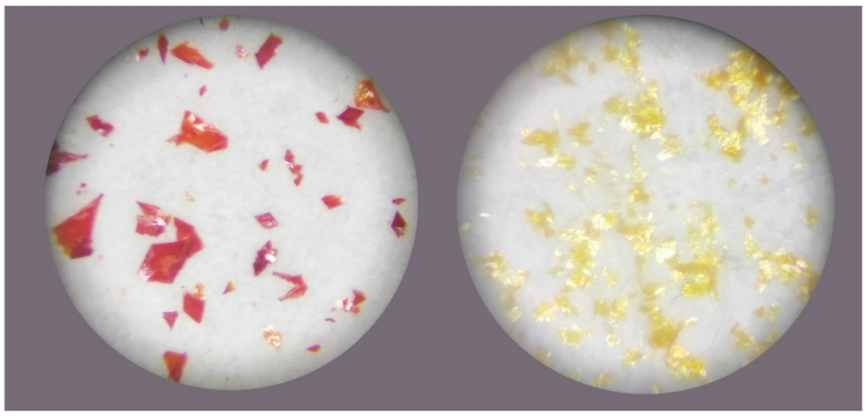

Fig. S1 Photograph of crystals of Pd_1Ag_{18} (left) and Pt_1Ag_{18} (right).

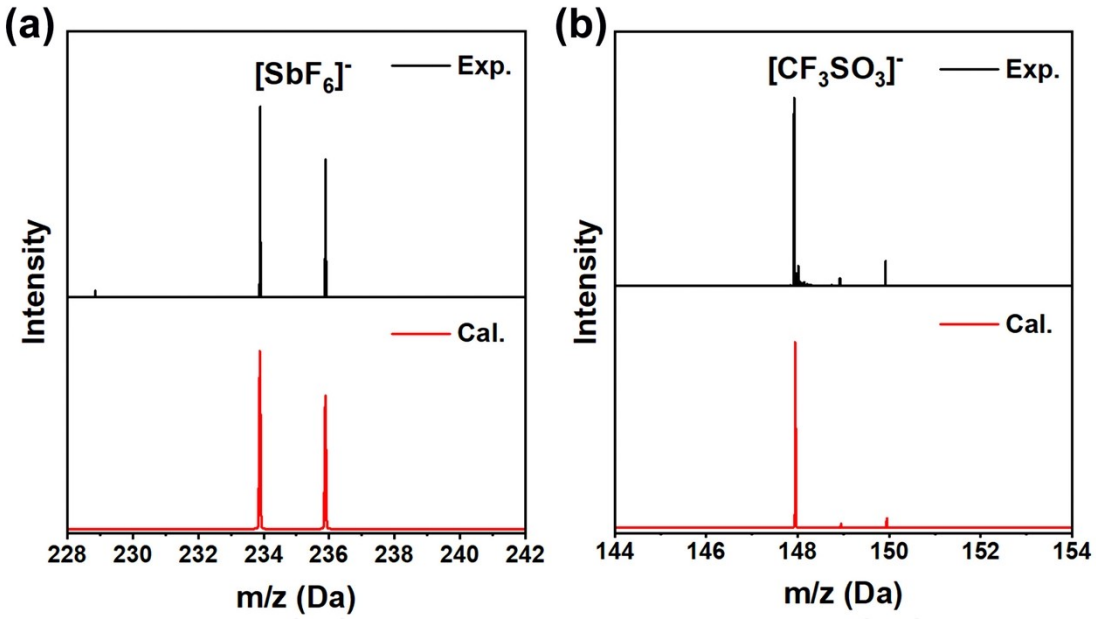

Fig. S2 ESI-MS spectra for Pd_1Ag_{18} (a) and Pt_1Ag_{18} (b) in the negative ion mode. Inset: experimental and simulated isotopic patterns for the SbF_6^- and $CF_3SO_3^-$ counterion peaks.

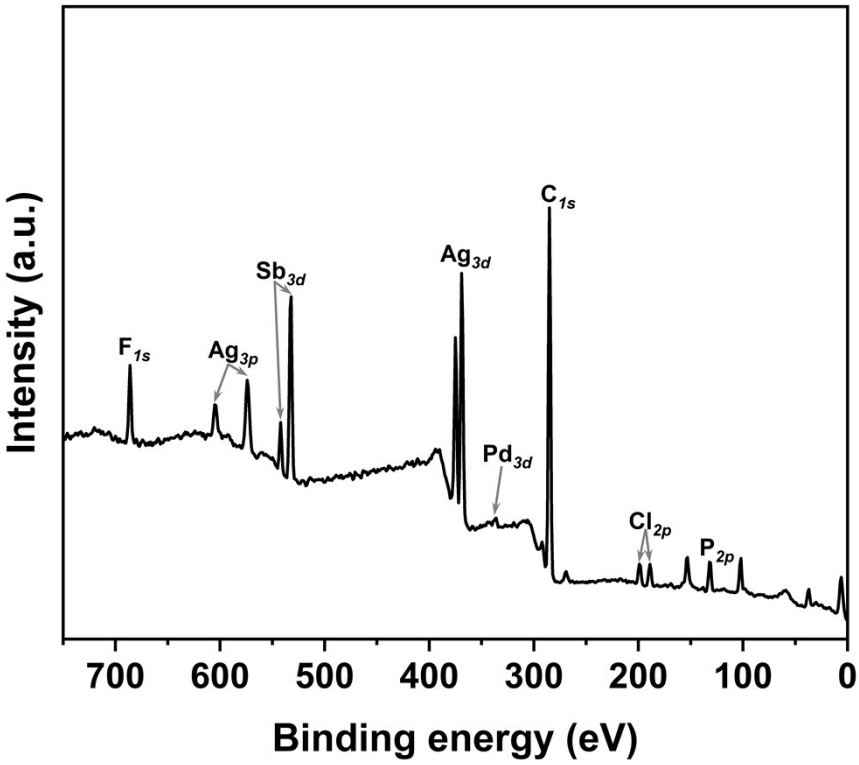

Fig. S3 The XPS survey of Pd_1Ag_{18}.

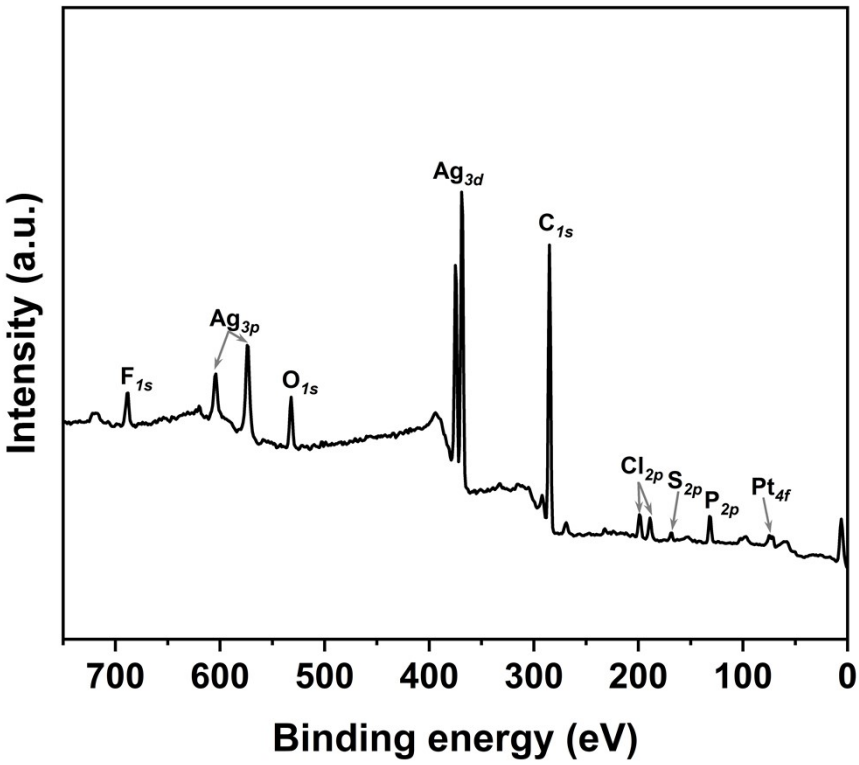

Fig. S4 The XPS survey of Pt_1Ag_{18}.

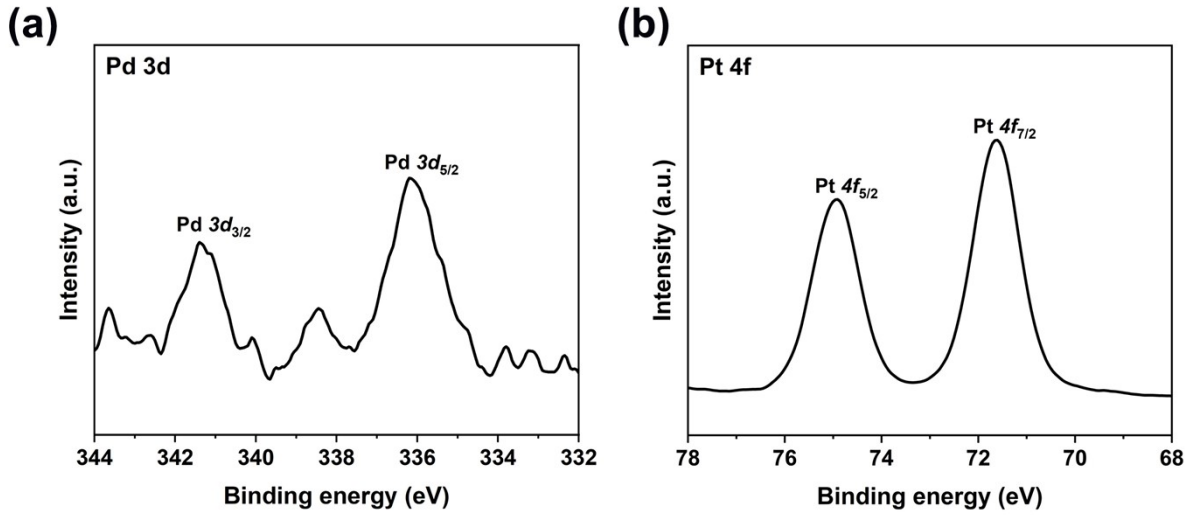

Fig. S5 The High-resolution XPS spectra of Pd *3d* (a) of Pd_1Ag_{18} and Pt *4f* (b)of Pt_1Ag_{18}.

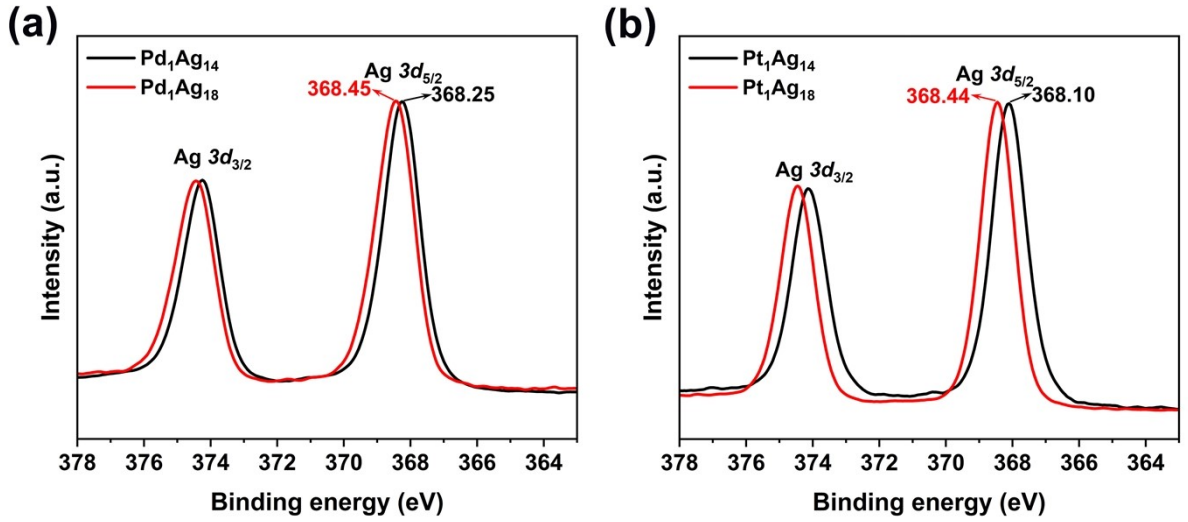

Fig. S6 The High-resolution XPS spectra of Ag *3d* of M_1Ag_{14} (black trace) and M_1Ag_{18} (red trace).

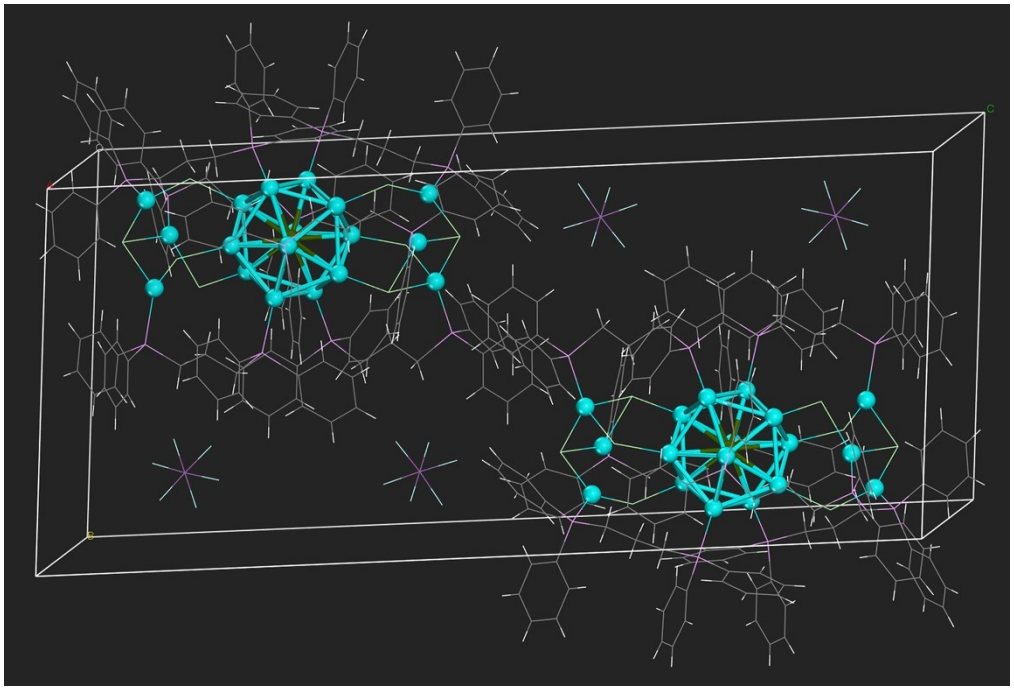

Fig. S7 The molecules packing diagrams of Pd_1Ag_{18} in one unit cell. Atom colors: dark green, Pd; sky blue, Ag; purple, Sb; bright green, Cl; cyan, F; magenta, P; gray, C; white, H.

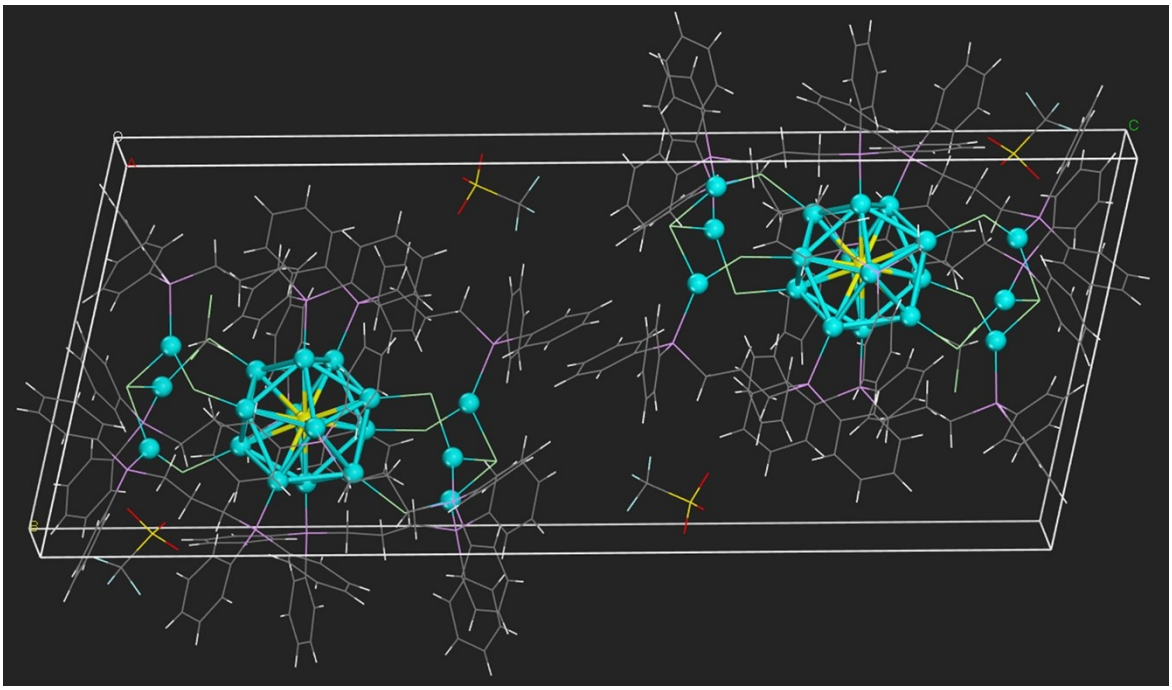

Fig. S8 The molecules packing diagrams of Pt_1Ag_{18} in one unit cell. Atom colors: bright yellow, Pt; sky blue, Ag; bright green, Cl; cyan, F; red, O; dark yellow, S; magenta, P; gray, C; white, H.

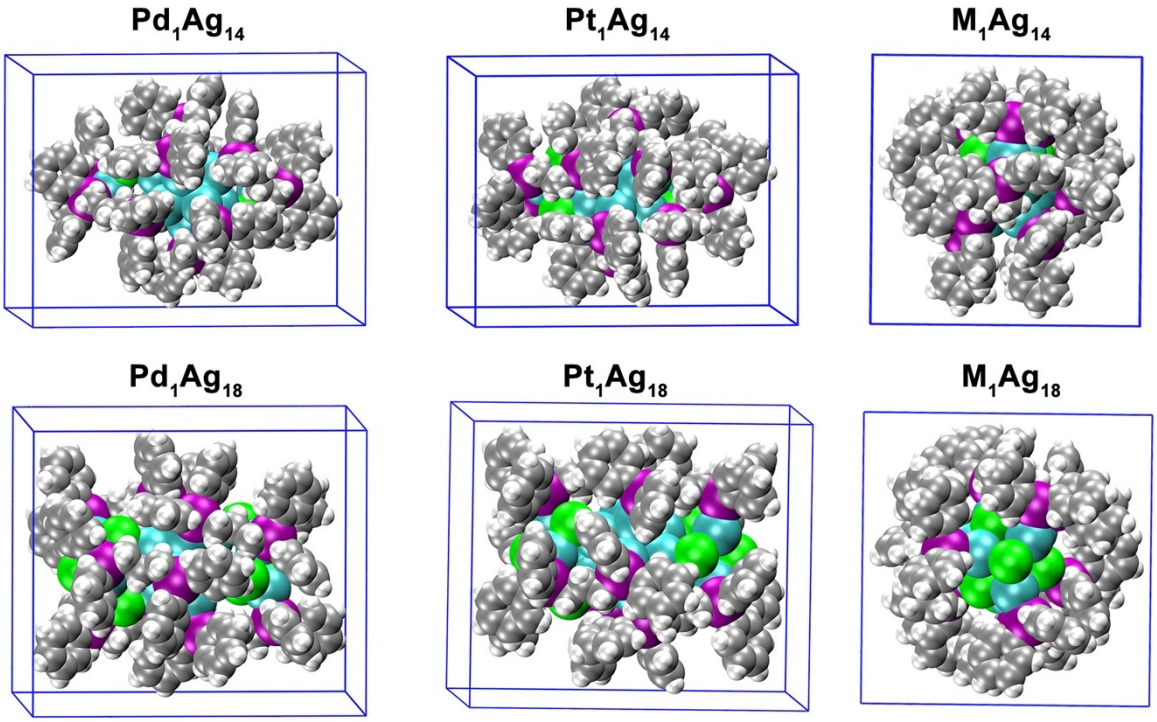

Fig. S9 Structure of M_1Ag_{18} and M_1Ag_{18} (M = Pd, Pt) shown as a space-filling model, viewed from different perspectives.

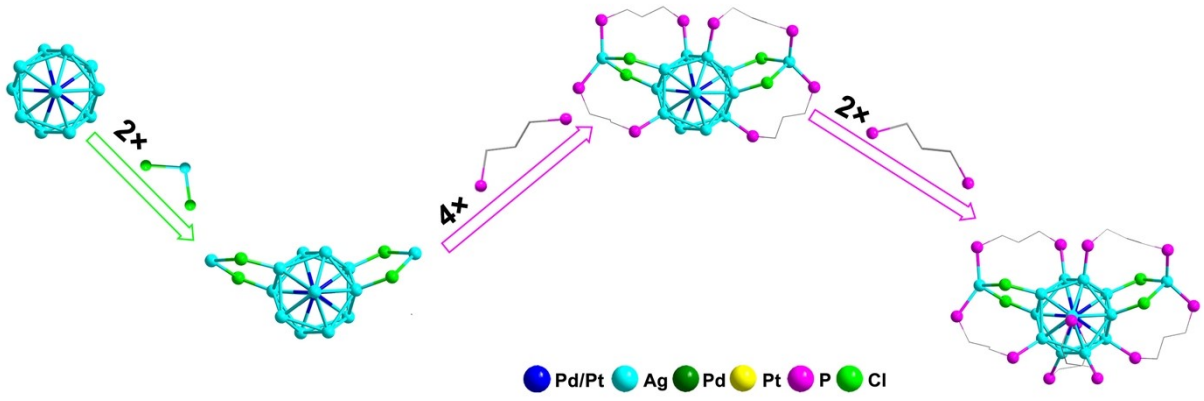

Fig. S10 Structure anatomy of M_1Ag_{14} (M = Pd, Pt) clusters. Color codes: blue, Pd or Pt; dark green, Pd; yellow, Pt; sky blue, Ag; bright green, Cl; magenta, P. For the sake of clarity, H and benzene are omitted.

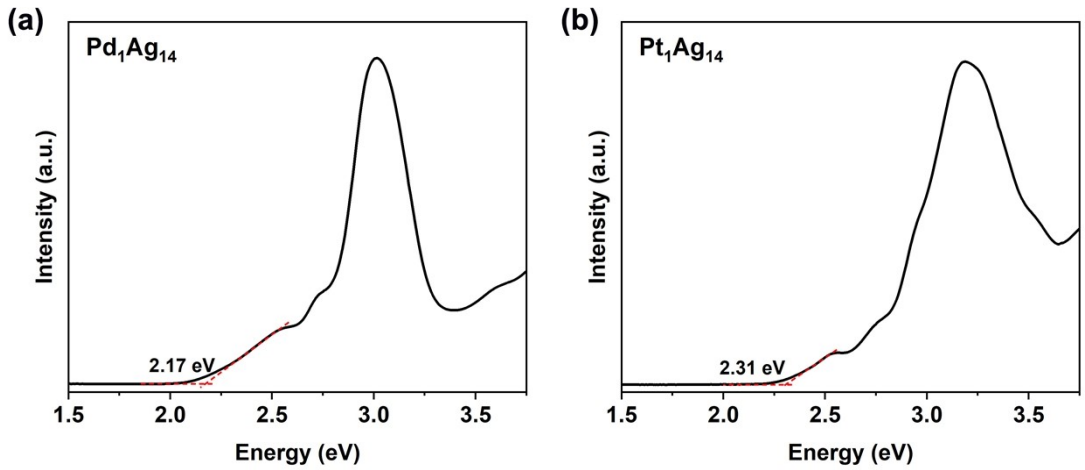

Fig. S11 The absorption spectra of Pd_1Ag_{14} (a) and Pt_1Ag_{14} (b) on an energy scale.

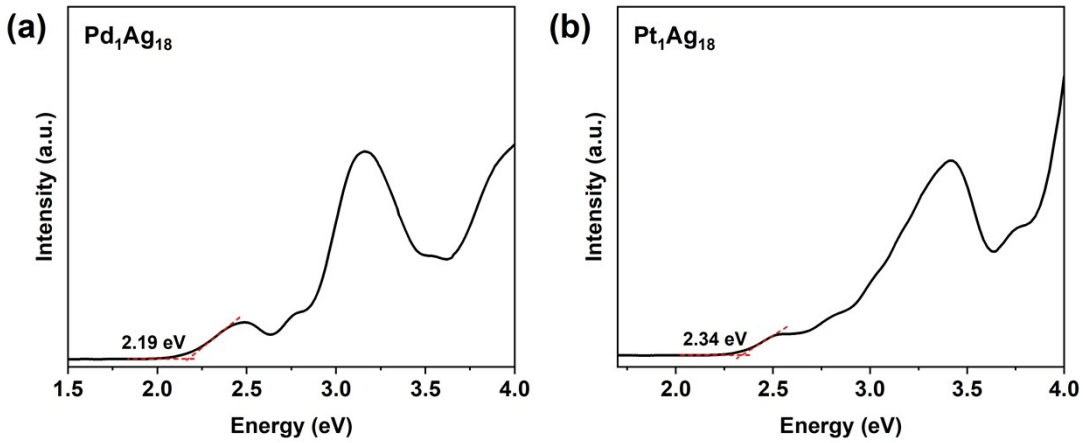

Fig. S12 The absorption spectra of Pd_1Ag_{18} (a) and Pt_1Ag_{18} (b) on an energy scale.

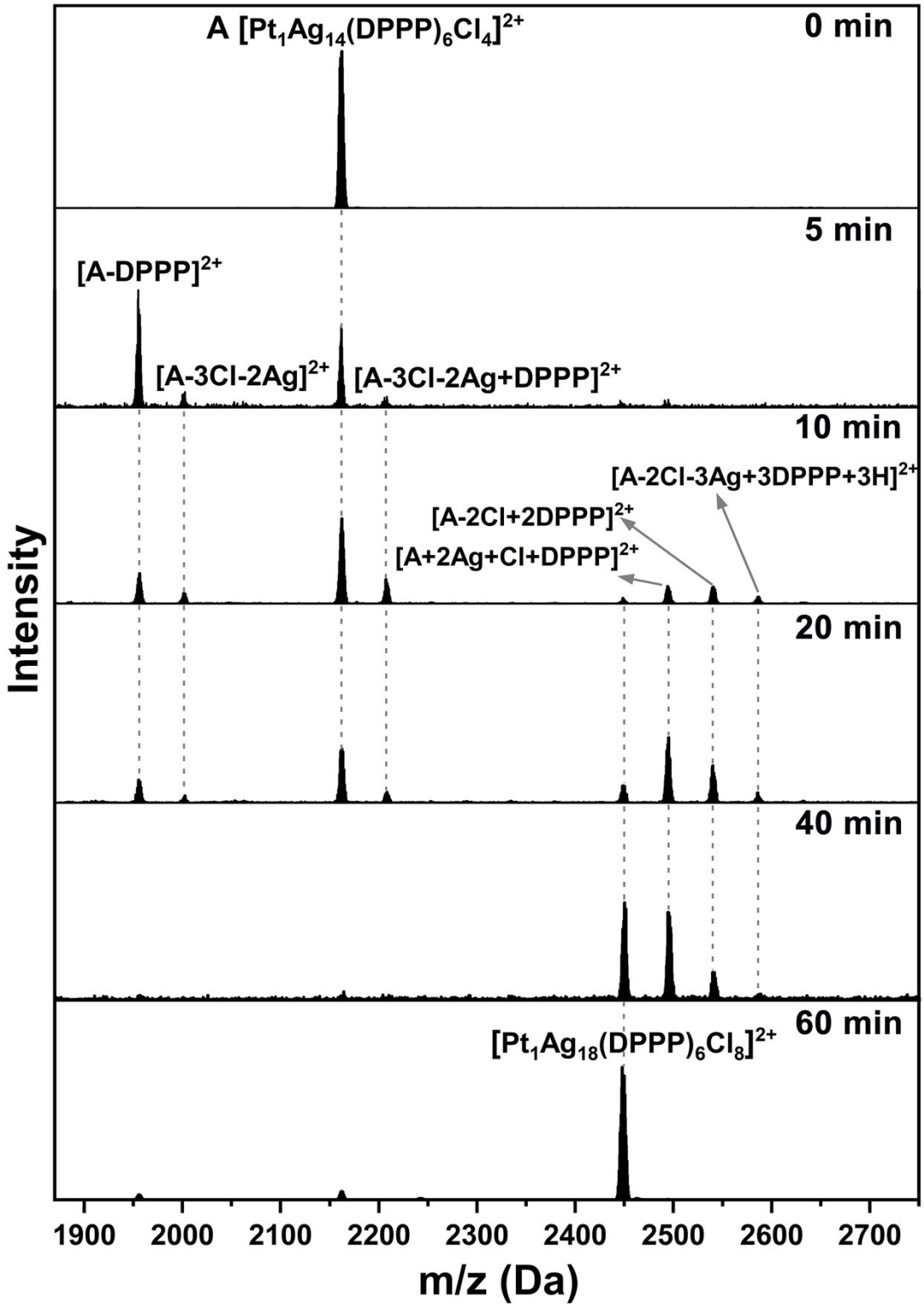

Fig. S13 ESI-MS tracking of the conversion from Pt_1Ag_{14} to Pt_1Ag_{18} under 365 nm light irradiation.

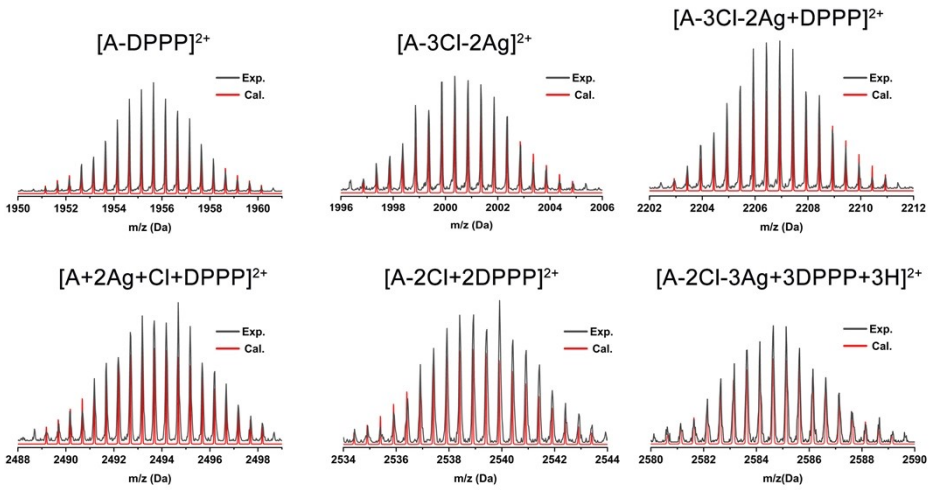

Fig. S14 Experimental (in black) and calculated (in red) isotope patterns for monitoring the formation of intermediates from Pt_1Ag_{14} during light exposure.

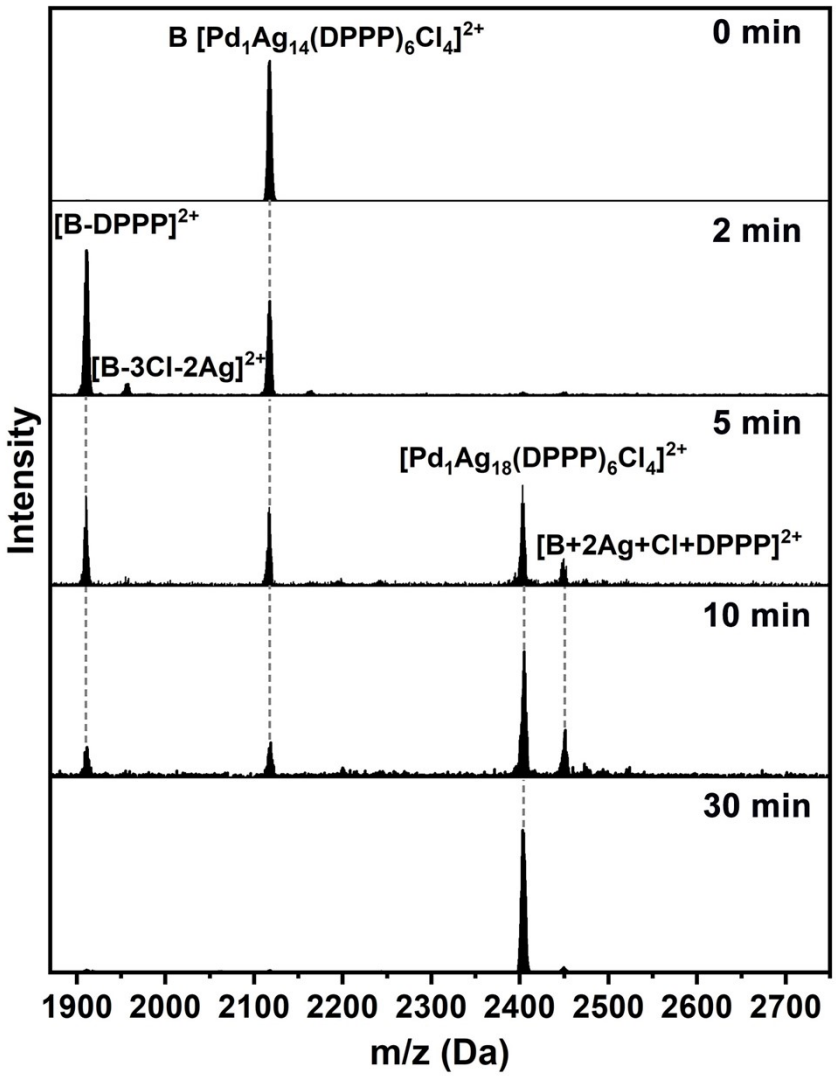

Fig. S15 ESI-MS tracking of the conversion from Pd_1Ag_{14} to Pd_1Ag_{18} under 365 nm light irradiation.

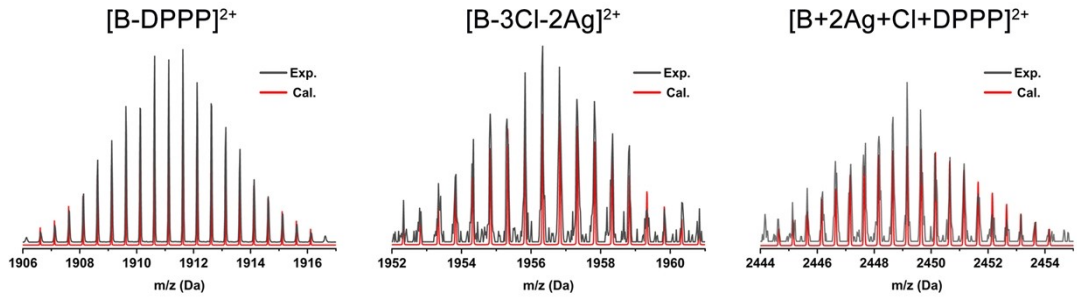

Fig. S16 Experimental (in black) and calculated (in red) isotope patterns for monitoring the formation of intermediates from Pd_1Ag_{14} during light exposure.

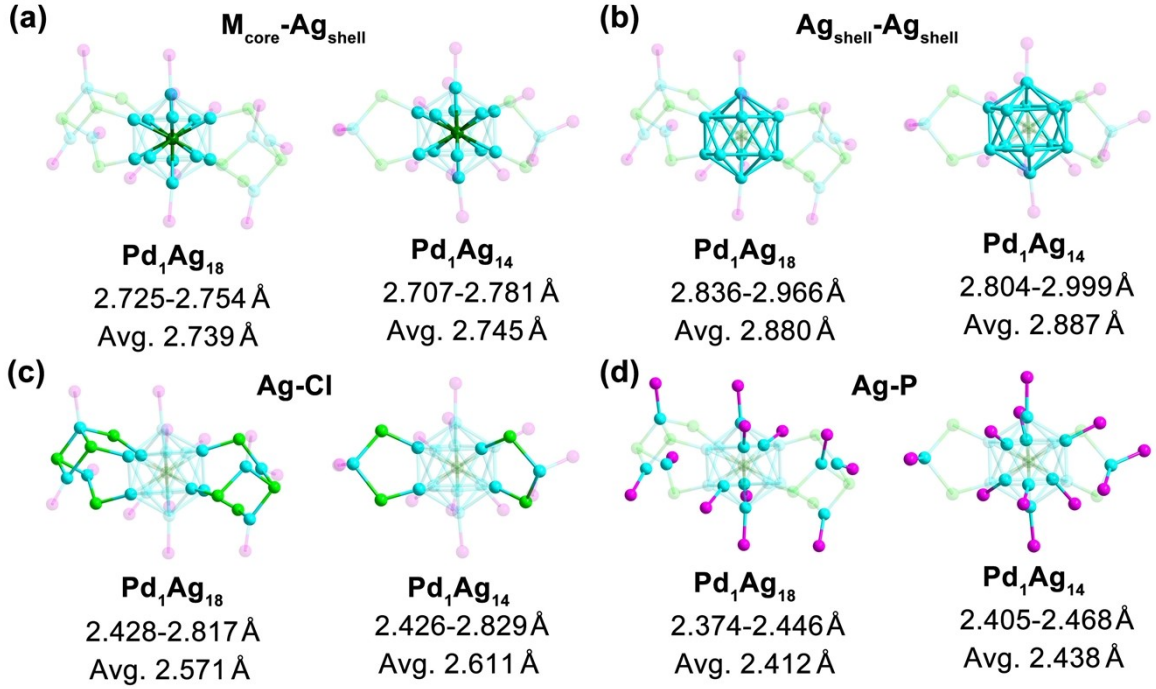

Fig. S17 Comparison of bond lengths of (a) M_{core}-Ag_{shell}, (b) Ag_{shell}-Ag_{shell}, (c) Ag-Cl, and (d) Ag-P between Pd_1Ag_{14} and Pd_1Ag_{18} NCs. The compared bonds are highlighted. Color code: dark green, Pd; sky blue, Ag; bright green, Cl; magenta, P.

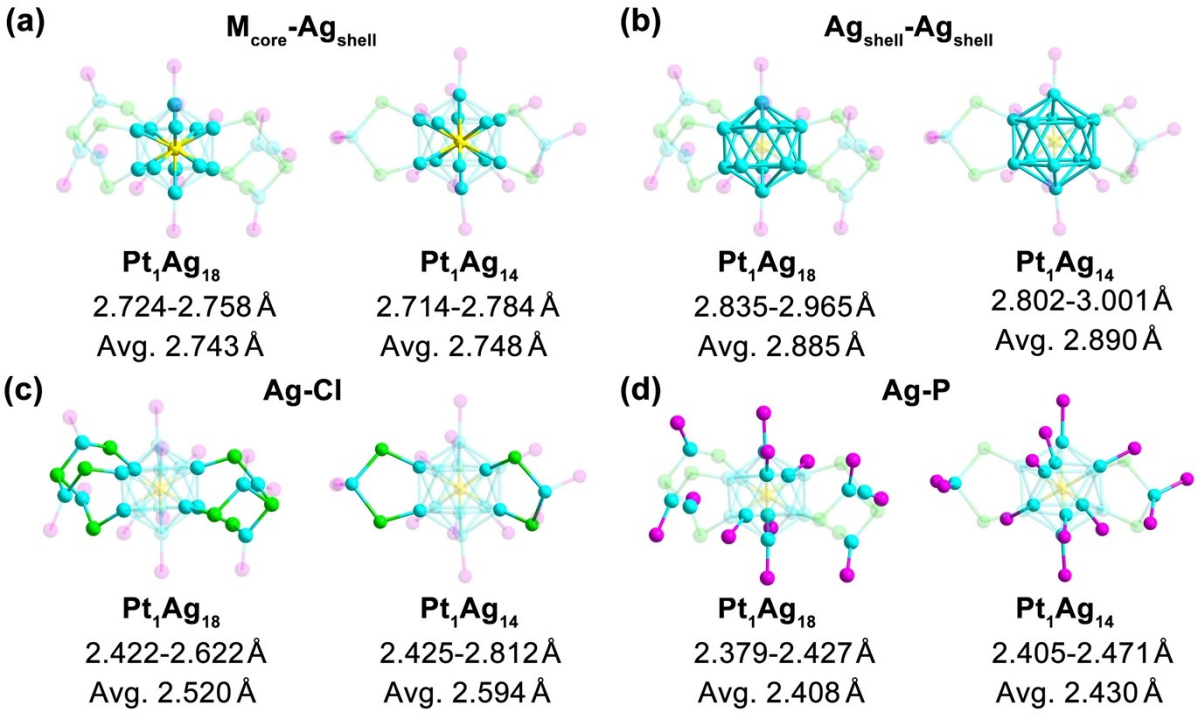

Fig. S18 Comparison of bond lengths of (a) M_{core}-Ag_{shell}, (b) Ag_{shell}-Ag_{shell}, (c) Ag-Cl, and (d) Ag-P between Pt_1Ag_{14} and Pt_1Ag_{18} NCs. The compared bonds are highlighted. Color code: yellow, Pt; sky blue, Ag; bright green, Cl; magenta, P.

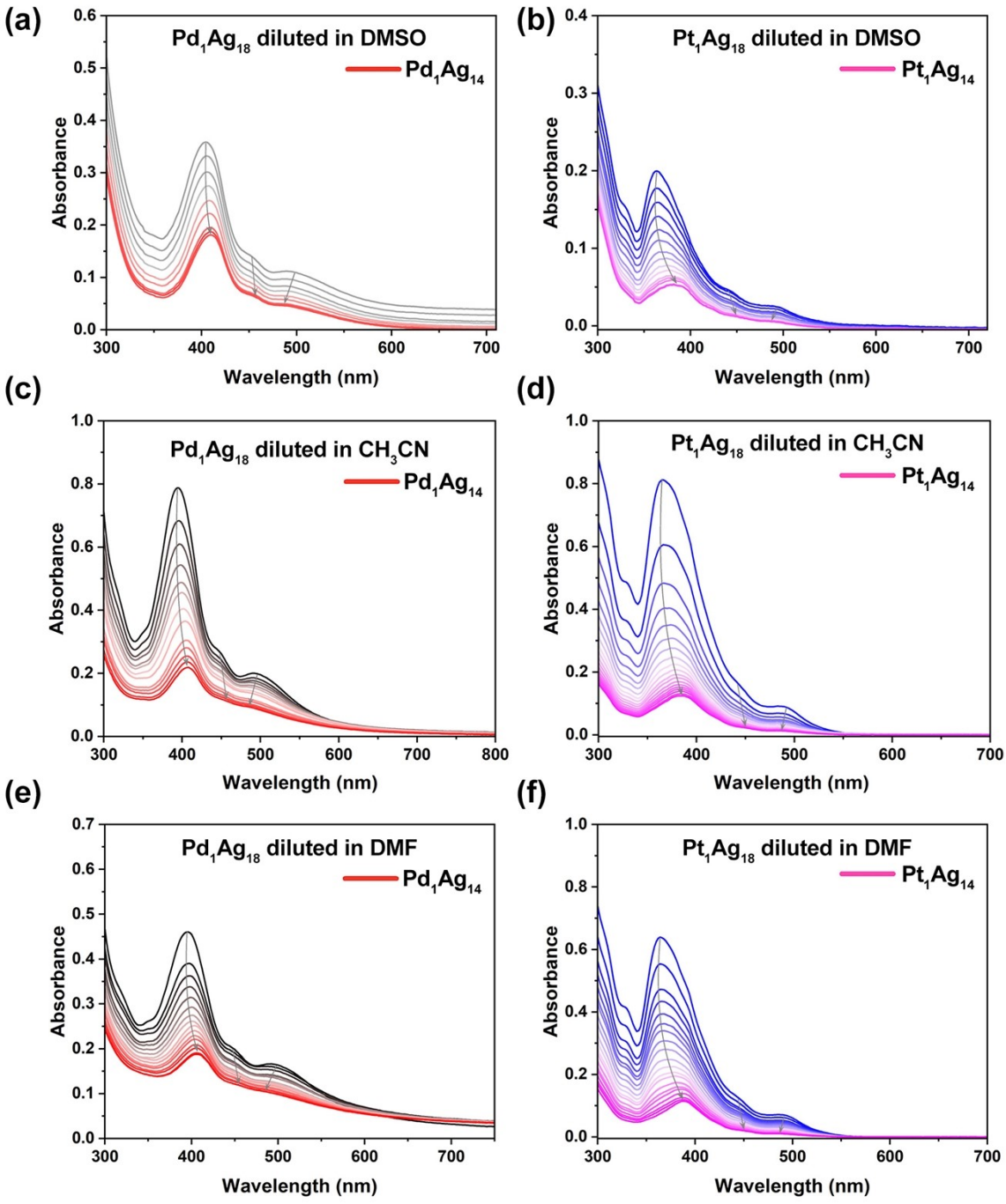

Fig. S19 UV−Vis spectra of Pt_1Ag_{18} and Pd_1Ag_{18} crystals dissolved and diluted in polar solvents: DMSO (a, b), CH_3CN (c, d), and DMF (e, f). A rather fast transformation was observed for Pd_1Ag_{18} upon its initial dissolution in DMSO. And these polar solvents induce the transformation from M_1Ag_{18} to M_1Ag_{14}.

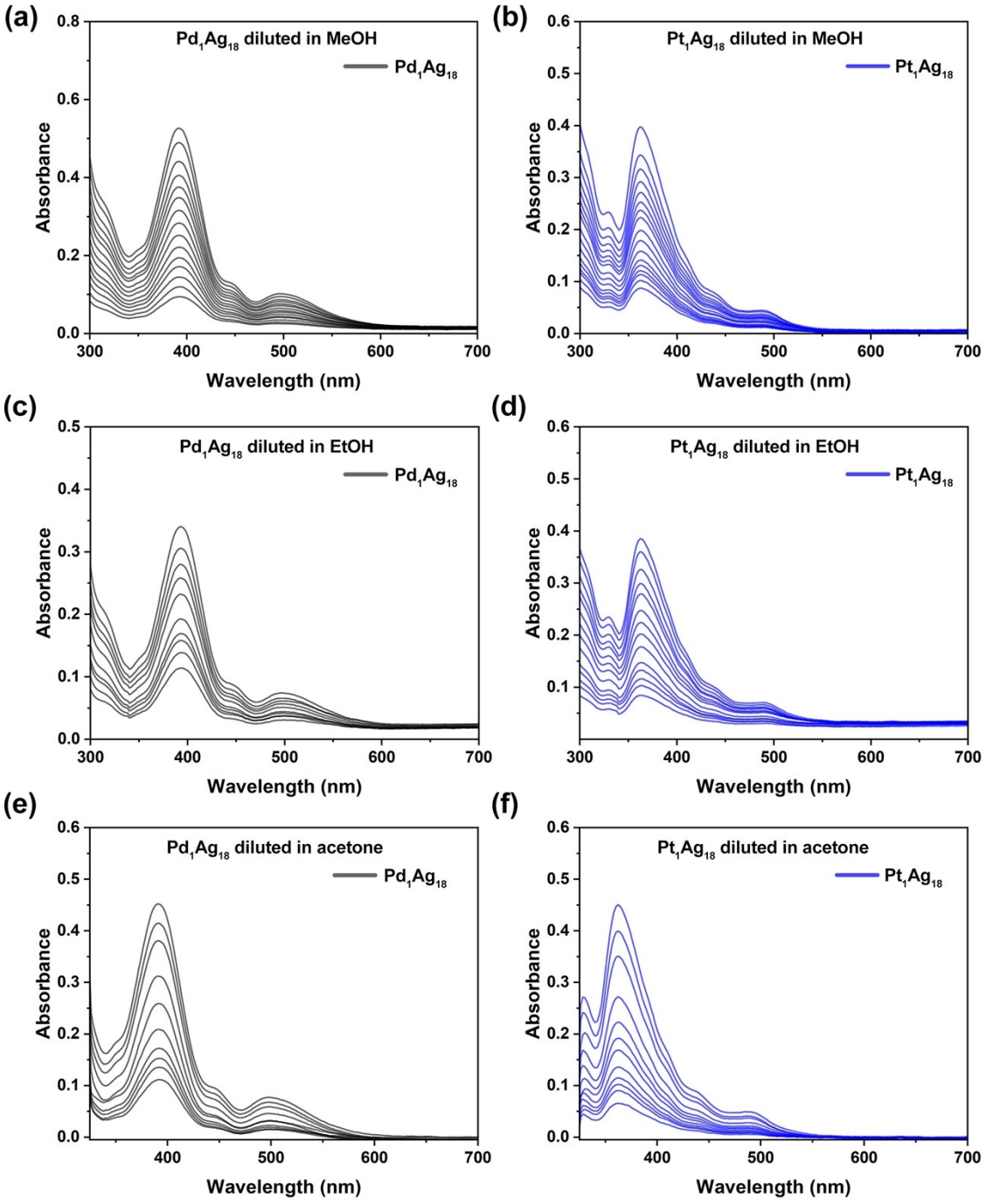

Fig. S20 UV−Vis spectra of Pt_1Ag_{18} and Pd_1Ag_{18} crystals dissolved and diluted in in less polar solvents: MeOH (a, b), EtOH (c, d), and acetone (e, f). These less polar solvents fail to induce the transformation from M_1Ag_{18} to M_1Ag_{14}.

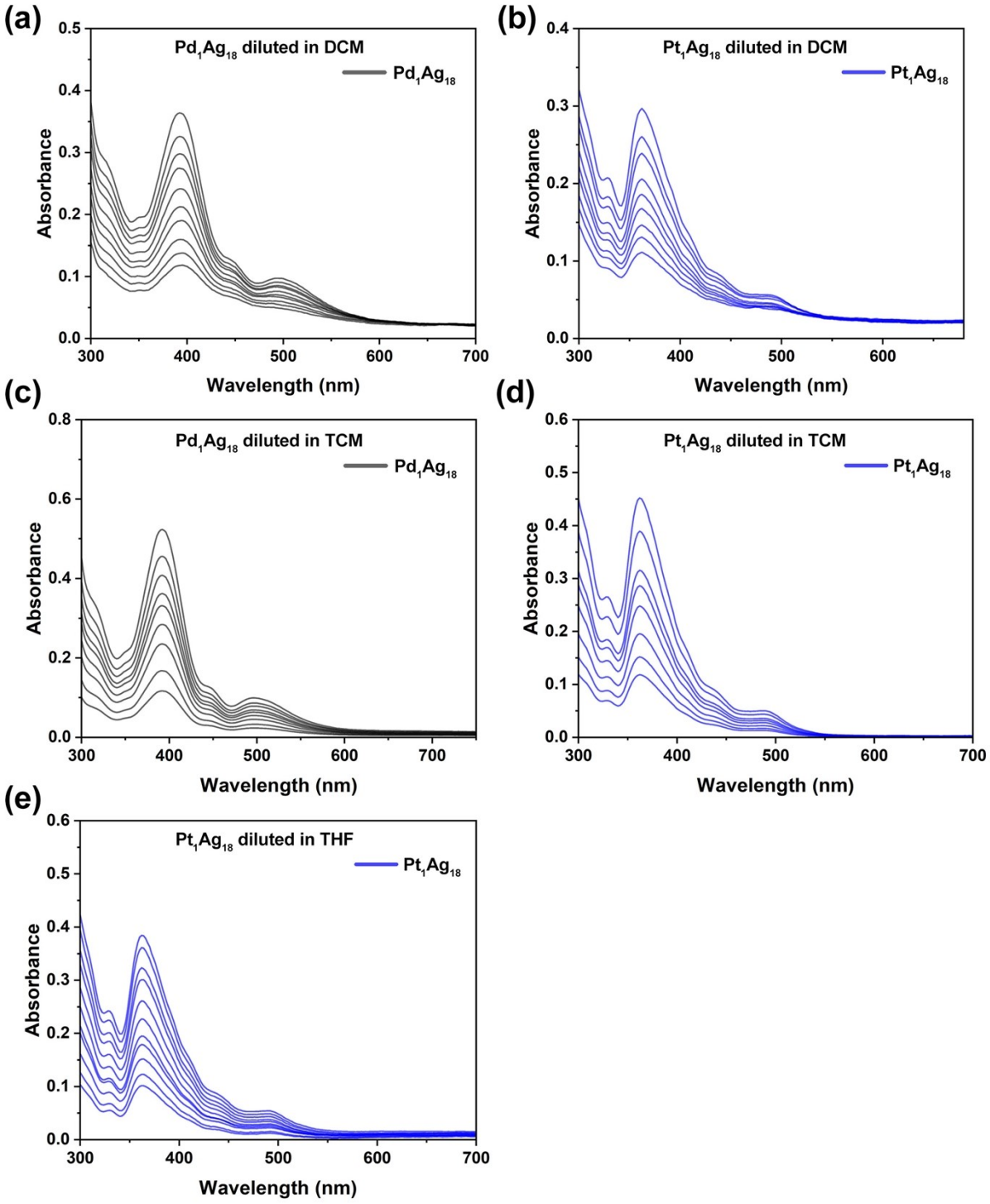

Fig. 21 UV−Vis spectra of Pt_1Ag_{18} and Pd_1Ag_{18} crystals dissolved and diluted in in less polar solvents: DCM (a, b), TCM (c, d), and THF (e). These weakly polar solvents cannot drive the conversion from M_1Ag_{18} to M_1Ag_{14}. And Pt_1Ag_{18} and Pd_1Ag_{18} crystals cannot dissolve in ethyl acetate. Additionally, Pd_1Ag_{18} is insoluble in THF, whereas Pt_1Ag_{18} is soluble, likely due to differences in the counterions (OTf^- for Pt_1Ag_{18} and SbF_6^- for Pd_1Ag_{18}).

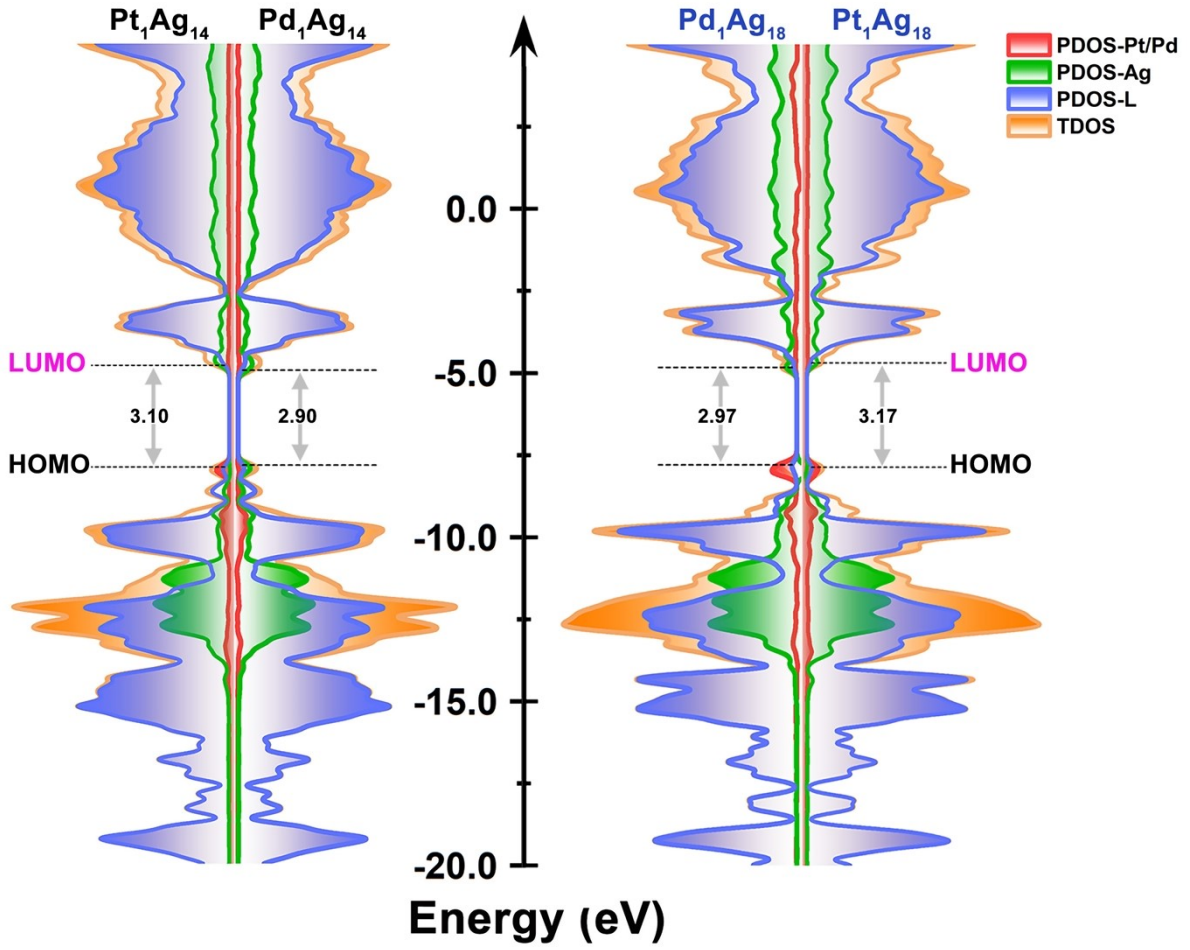

Fig. S22 Total and population partial density of states (DOS) of the optimized M_1Ag_{14} and M_1Ag_{18} (M=Pd, Pt), L represents the DPPP and Cl ligands.

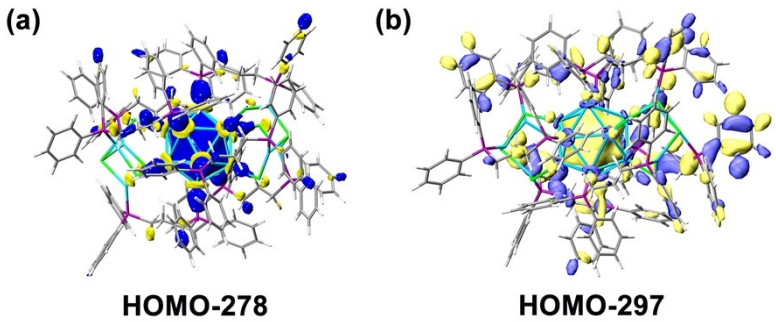

Fig. S23 Selected superatomic 1S orbital of HOMO-278 in Pd_1Ag_{18} and HOMO-297 in Pt_1Ag_{18} nanocluster.

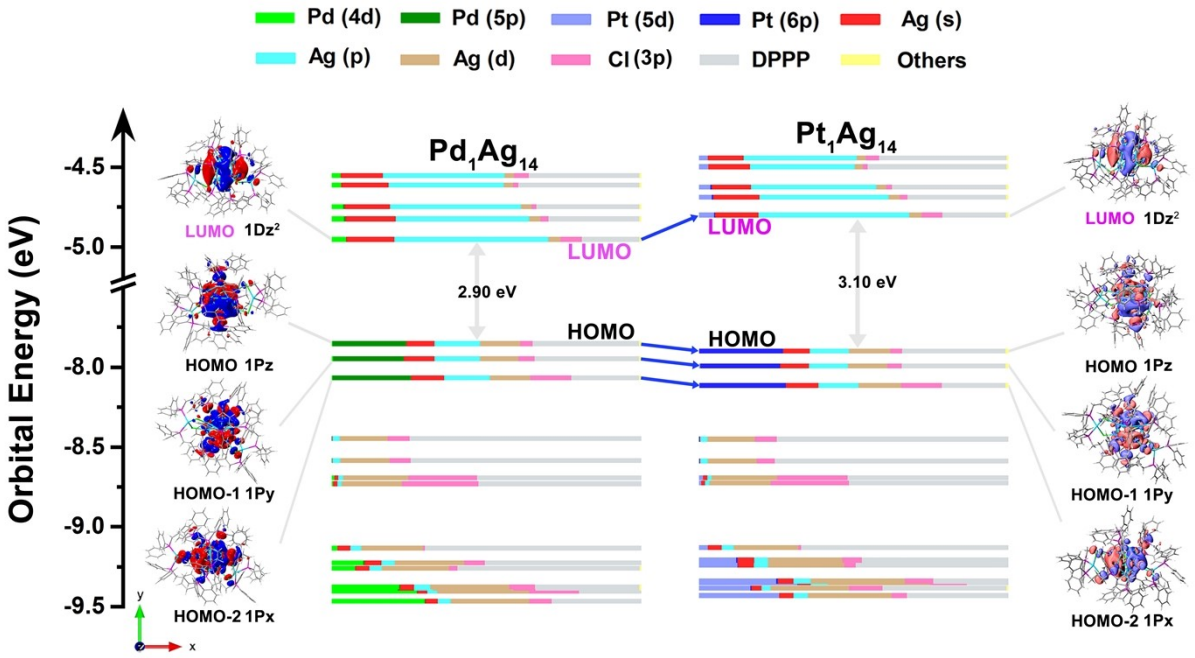

Fig. S24 Comparison of the Kohn-Sham molecular orbital diagrams and orbital compositions between Pd_1Ag_{14} and Pt_1Ag_{14} clusters calculated at the B3LYP/def2-SVP level.

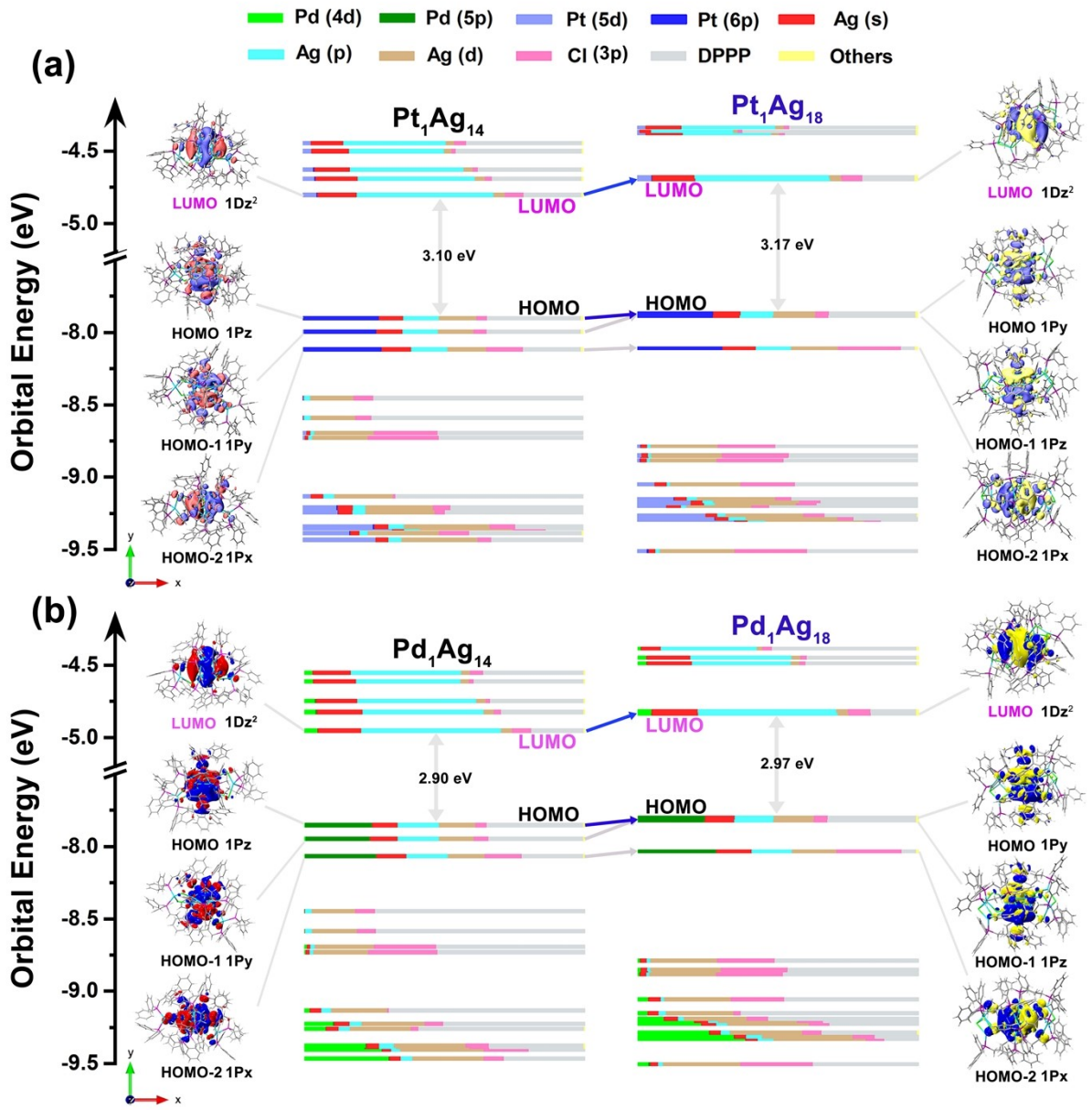

Fig. S25 Kohn−Sham molecular orbital energy level diagram and components of each orbital of M_1Ag_{14} and M_1Ag_{18} (M=Pd, Pt).

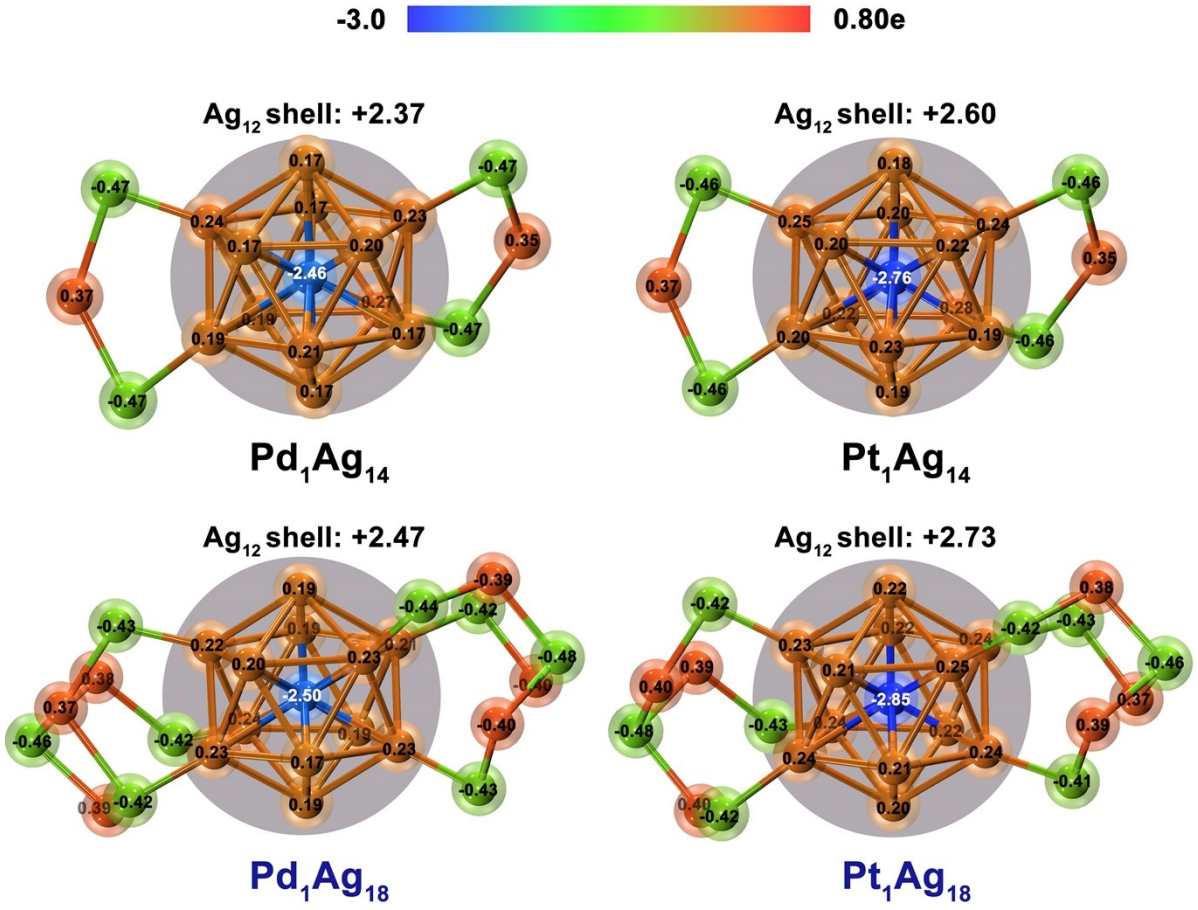

Fig. S26 Natural Population Analysis (NPA) charge distributions on the $M_1Ag_{14}Cl_4$ and $M_1Ag_{18}Cl_8$ unit of the lowest-energy structures of M_1Ag_{14} and M_1Ag_{18} (M = Pd, Pt).

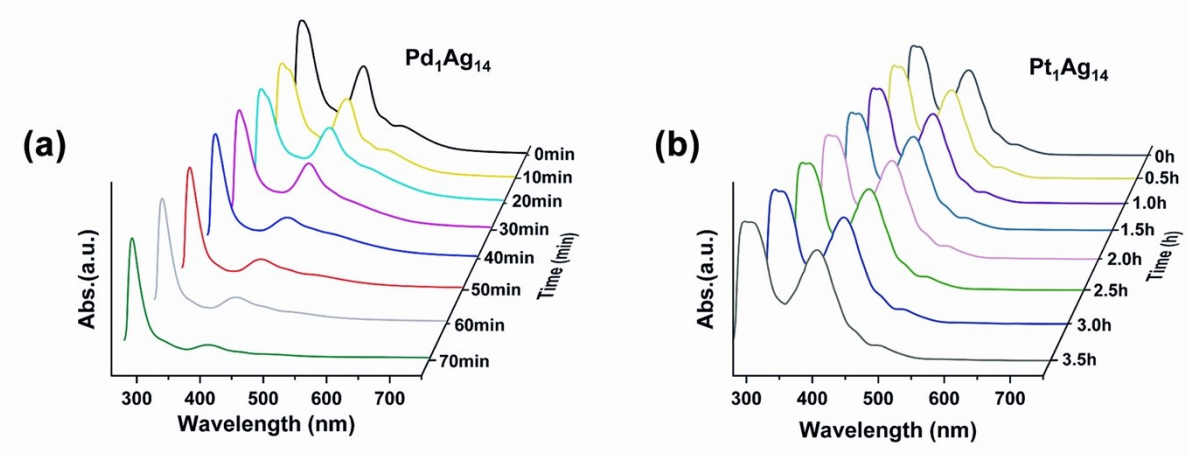

Fig. S27 The thermal stability of Pd_1Ag_{14} (a) and Pt_1Ag_{14} (b) in DMF under 60℃ monitored by UV-Vis spectrometry. The data for M_1Ag_{14} are from our previous work[1].

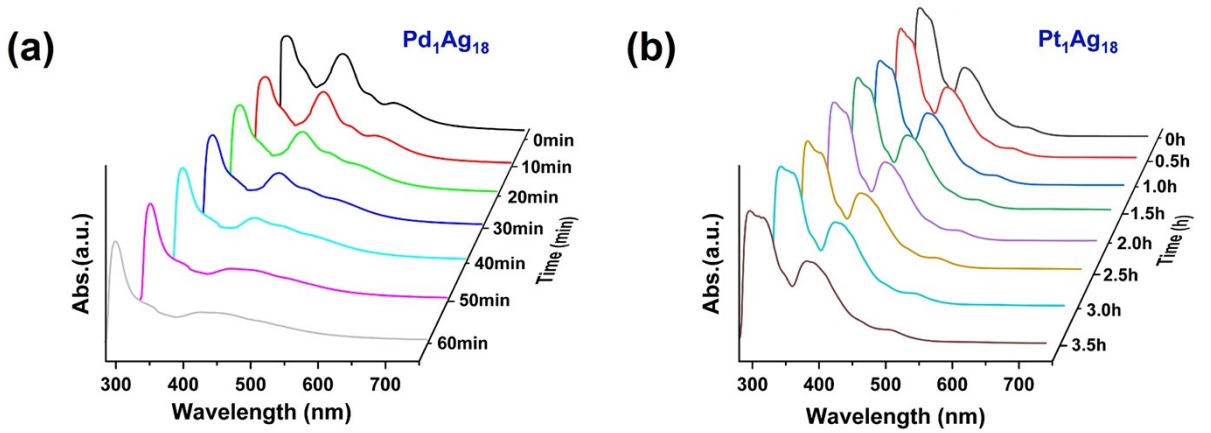

Fig. S28 The thermal stability of Pd_1Ag_{18} (a) and Pt_1Ag_{18} (b) in EtOH under 60℃ monitored by UV-Vis spectrometry.

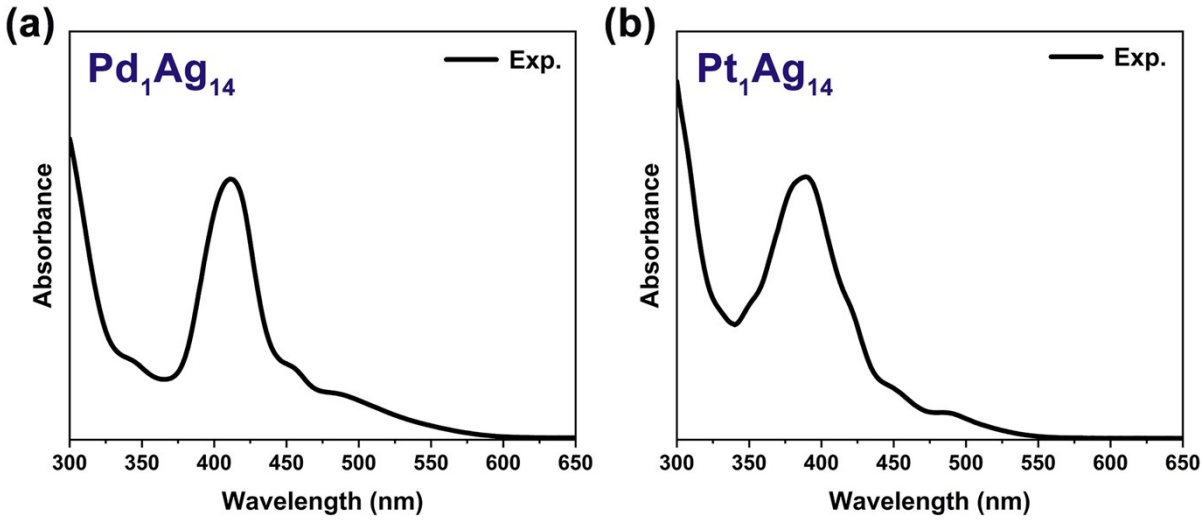

Fig. S29 The experimental UV–vis absorption spectra of M_1Ag_{14} (M = Pd, Pt) in DCM.

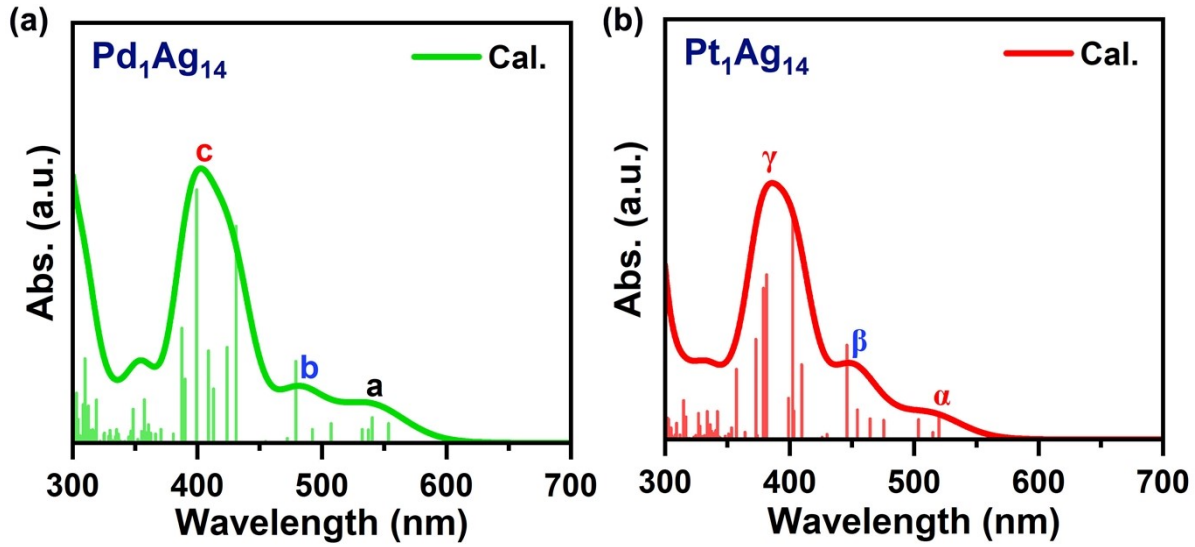

Fig. S30 The theoretical UV–Vis spectra of M_1Ag_{14} (M = Pd, Pt) calculation at B3LYP/def2-SVP level.

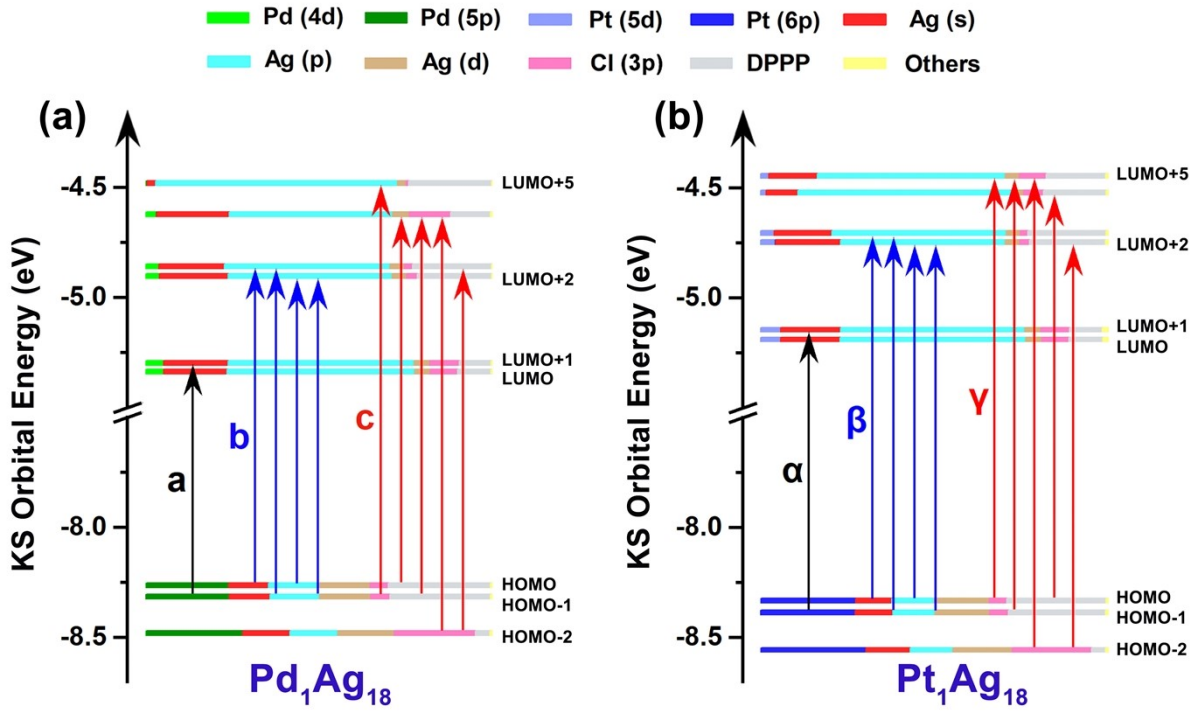

Fig. S31 The components of the Kohn-Sham orbitals of M_1Ag_{18} (M=Pd, Pt) and the vertical arrows correspond to likely optical transition.

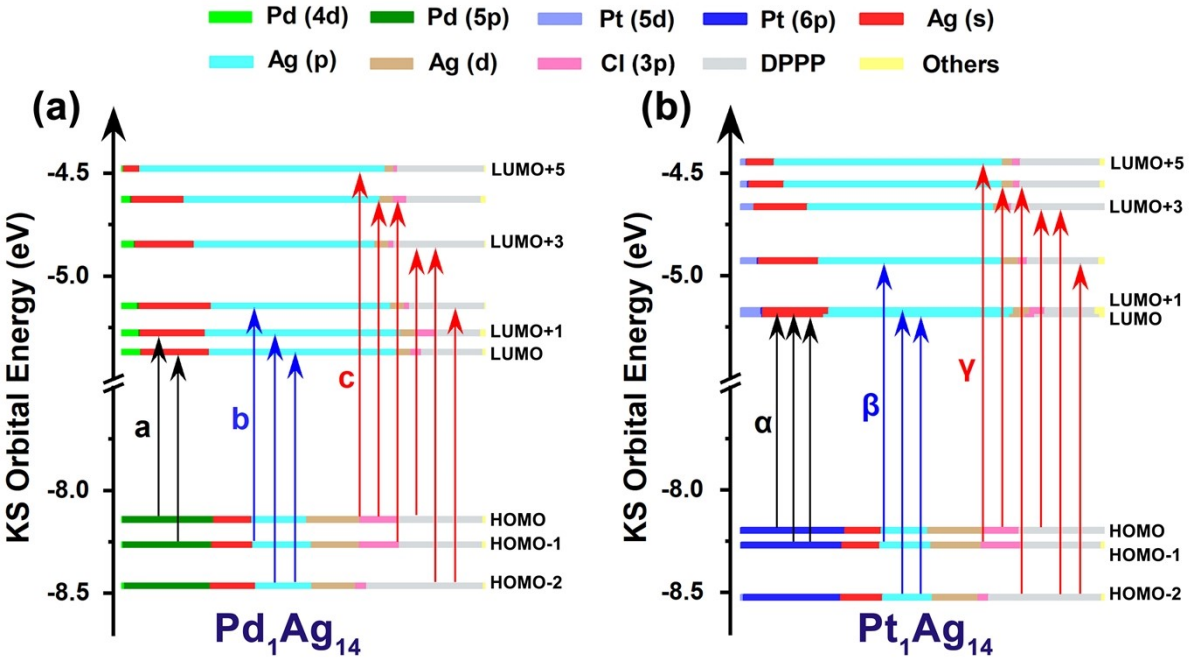

Fig. S32 The components of the Kohn-Sham orbitals of M_1Ag_{14} (M=Pd, Pt) and the vertical arrows correspond to likely optical transition.

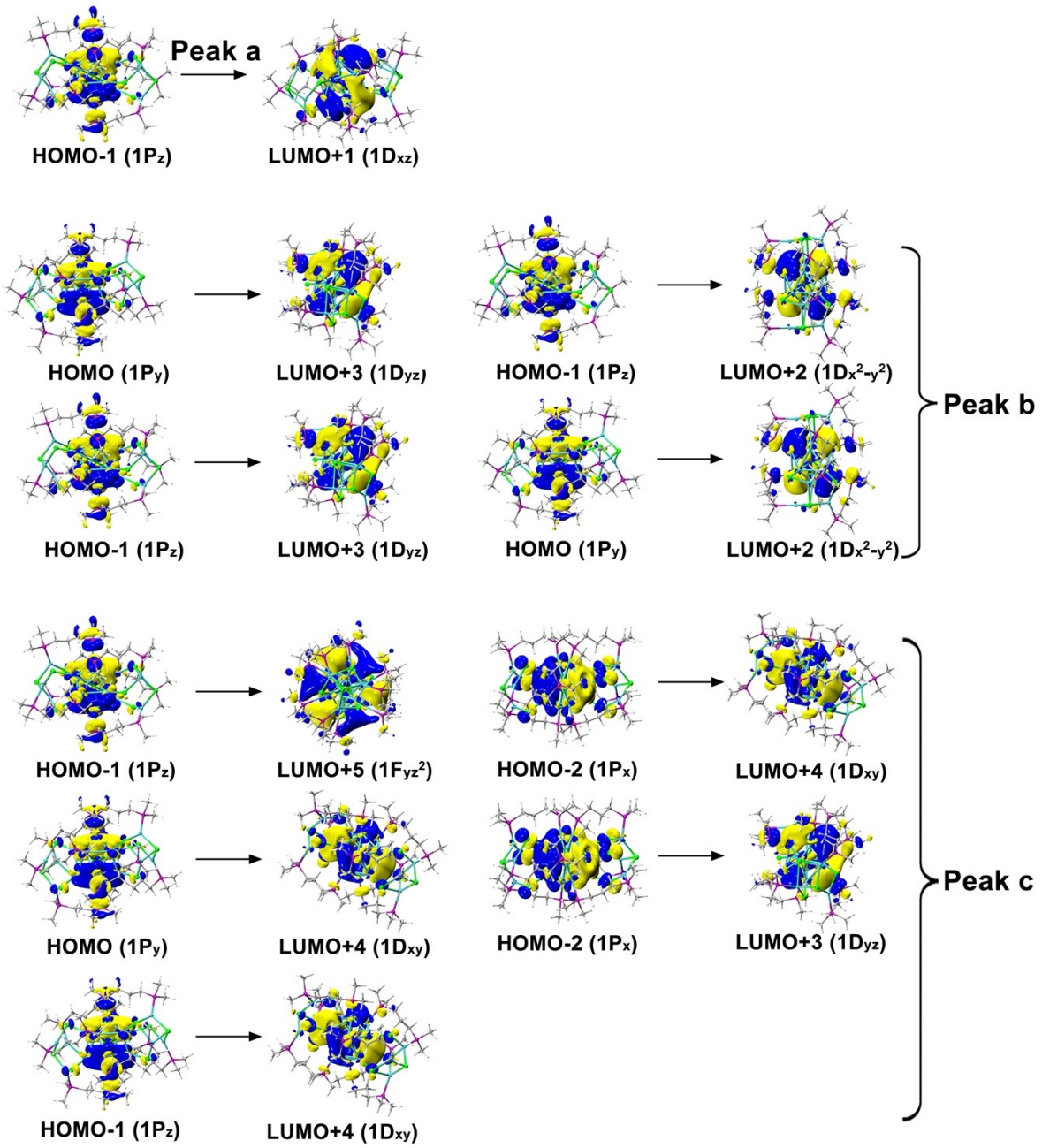

Fig. S33 Kohn–Sham orbitals relevant to the likely optical transitions in Pd_1Ag_{18}.

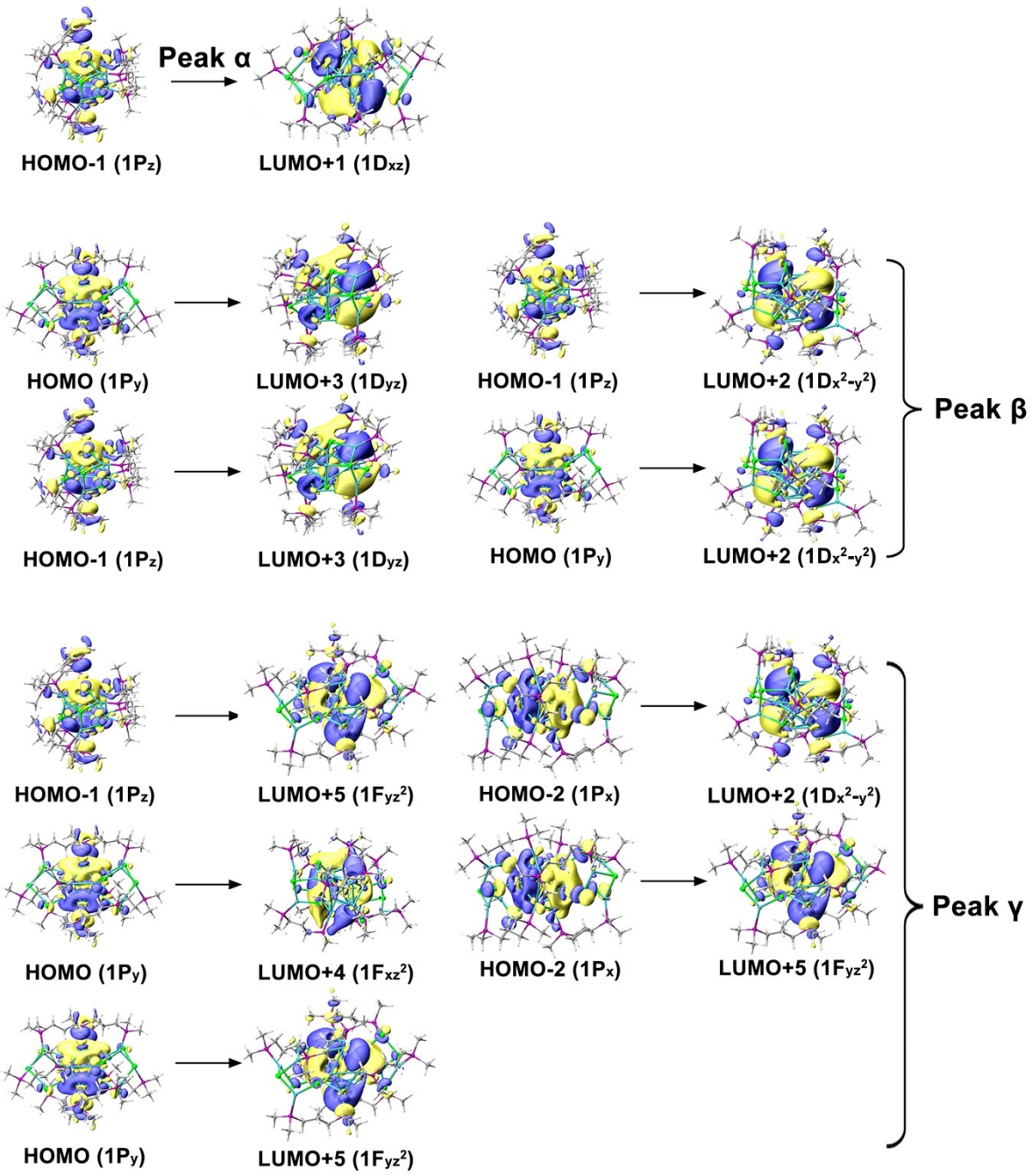

Fig. S34 Kohn–Sham orbitals relevant to the likely optical transitions in Pt_1Ag_{18}.

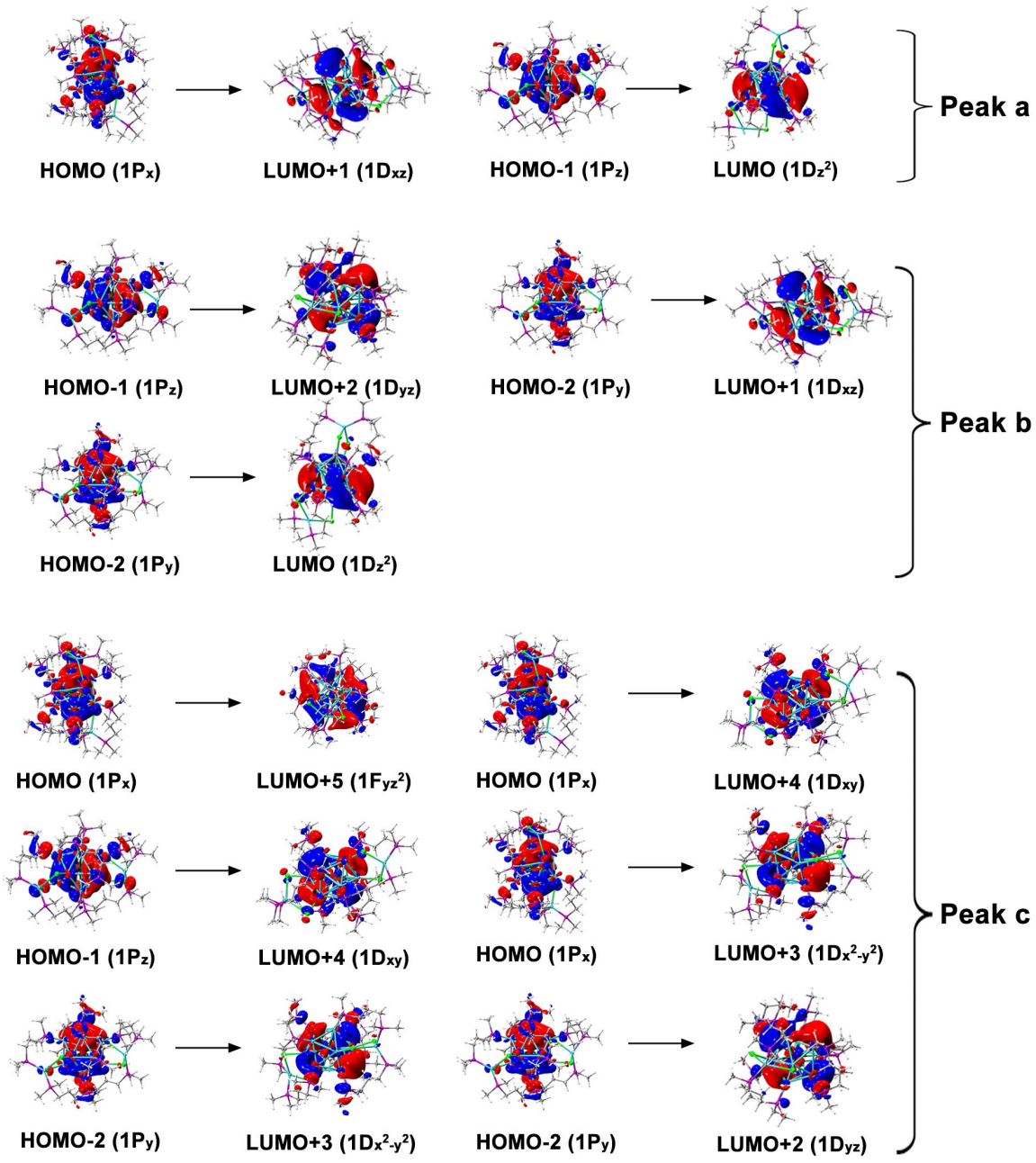

Fig. S35 Kohn–Sham orbitals relevant to the likely optical transitions in Pd_1Ag_{14}.

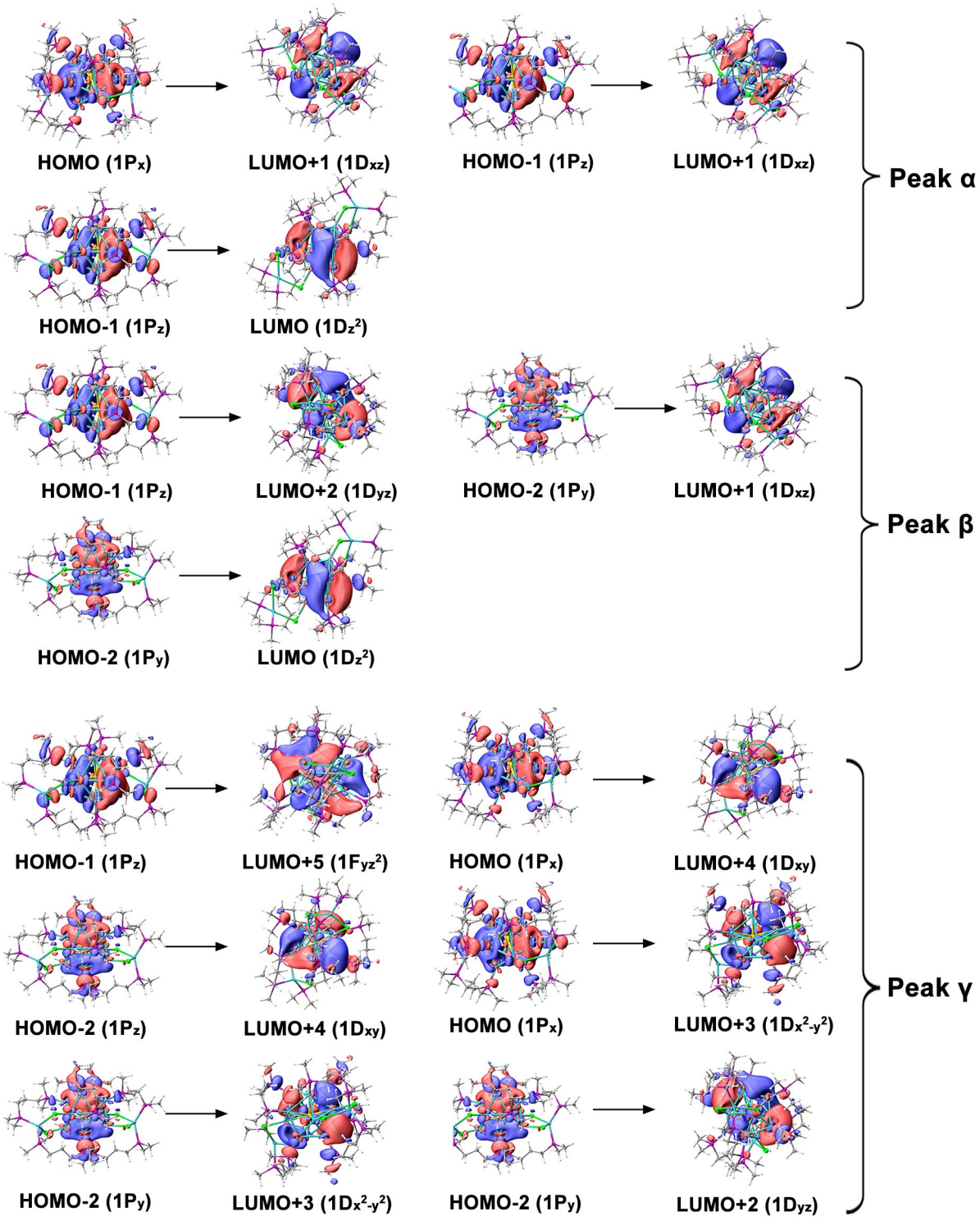

Fig. S36 Kohn–Sham orbitals relevant to the likely optical transitions in Pt_1Ag_{14}.

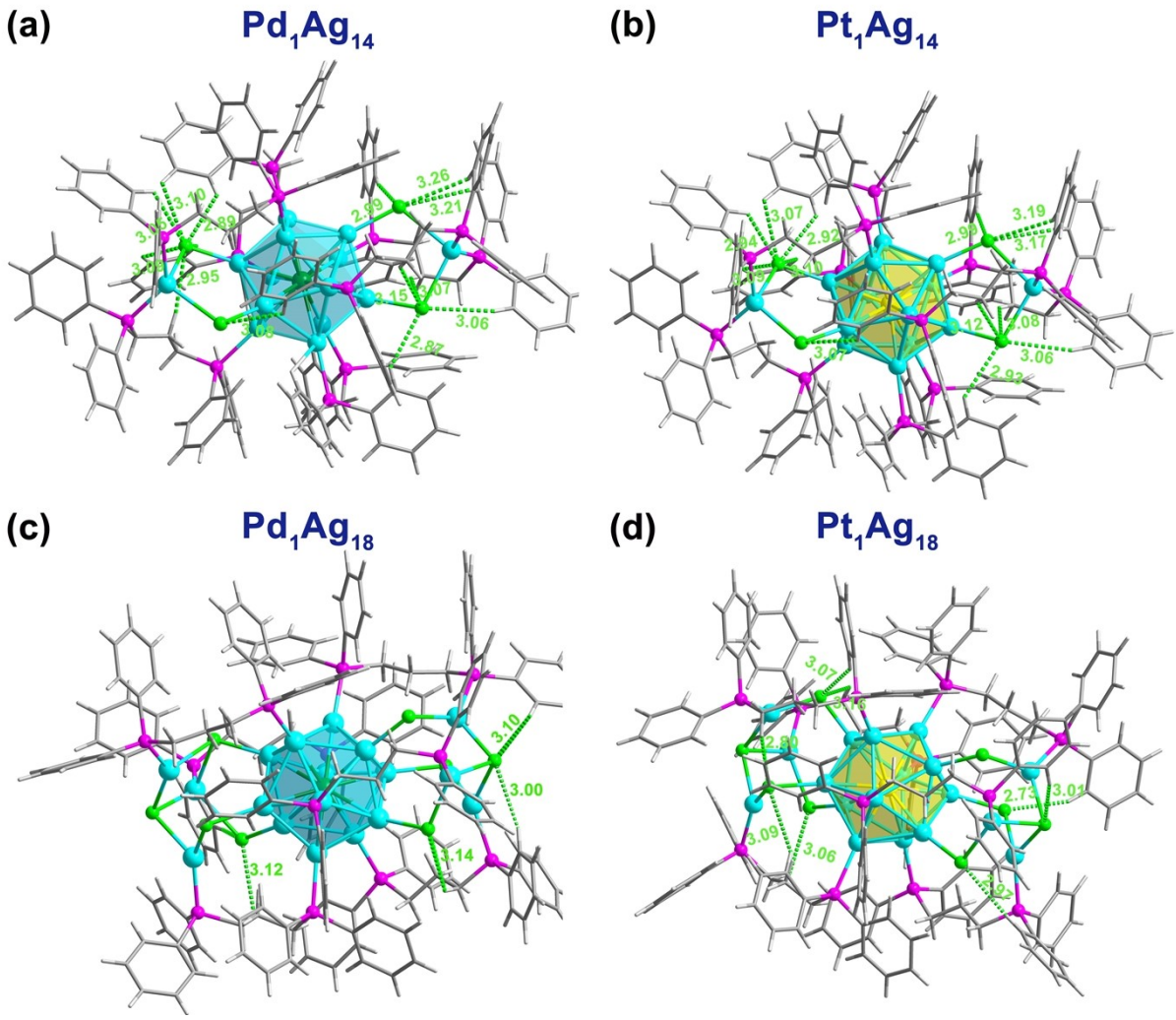

Fig. S37 Illustration of the intra-cluster non-covalent C-H···Cl interactions of M_1Ag_{14} (a, b) and M_1Ag_{18} (c, d) (M = Pd, Pt). The measured distances are indicated by dashed lines, and the blue numbers mark the distance between two planes in the intra-cluster parallel-displaced π···π interactions. Color code: dark green, Pd; yellow, Pt; sky blue, Ag; bright green, Cl; magenta, P; gray, C and white, H.

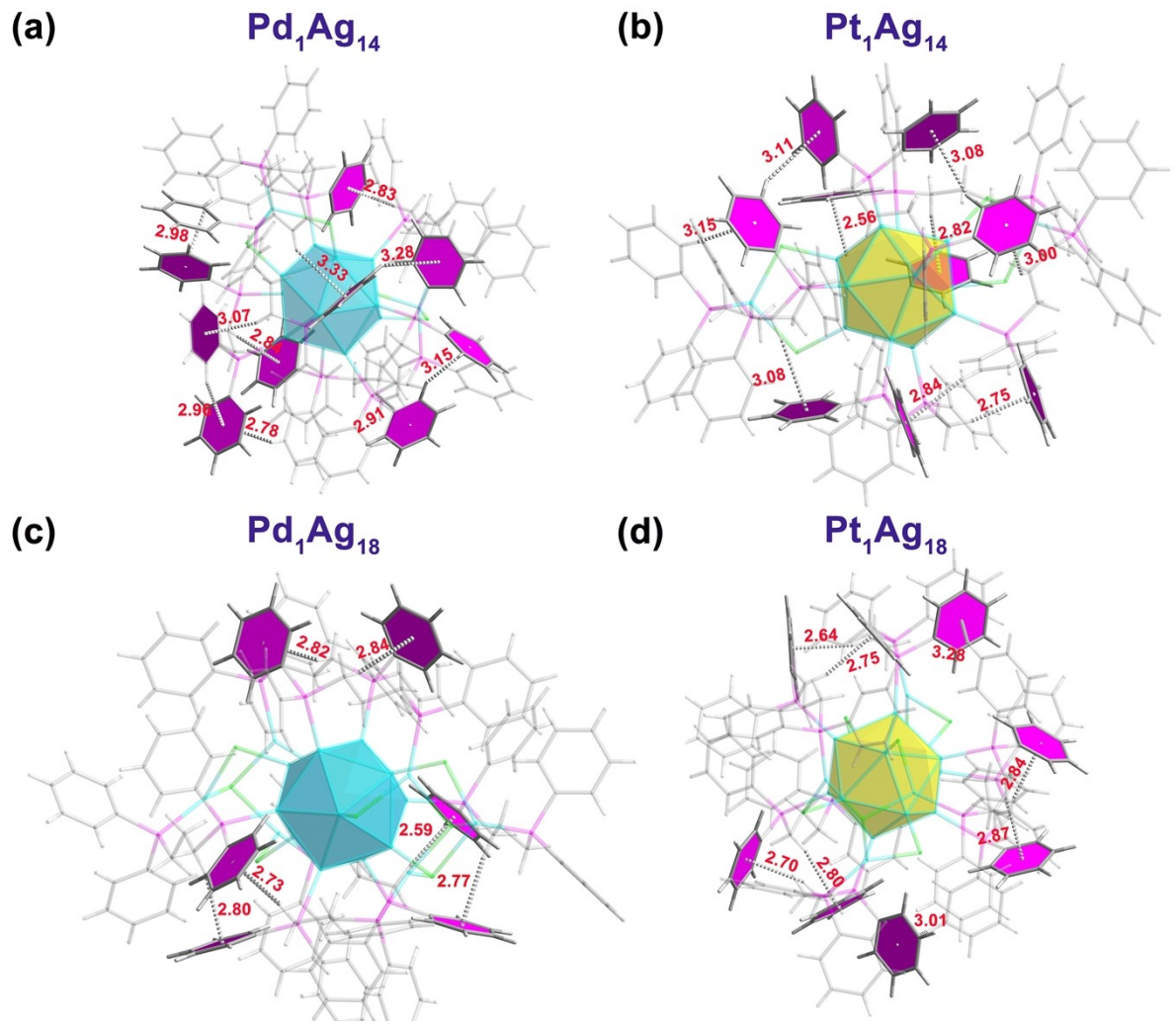

Fig. S38 Illustration of the intra-cluster non-covalent C-H···π interactions of M_1Ag_{14} (a, b) and M_1Ag_{18} (c, d) (M = Pd, Pt). The measured distances are indicated by dashed lines, and the blue numbers mark the distance between two planes in the intra-cluster parallel-displaced π···π interactions. Color code: dark green, Pd; yellow, Pt; sky blue, Ag; bright green, Cl; magenta, P; gray, C and white, H.

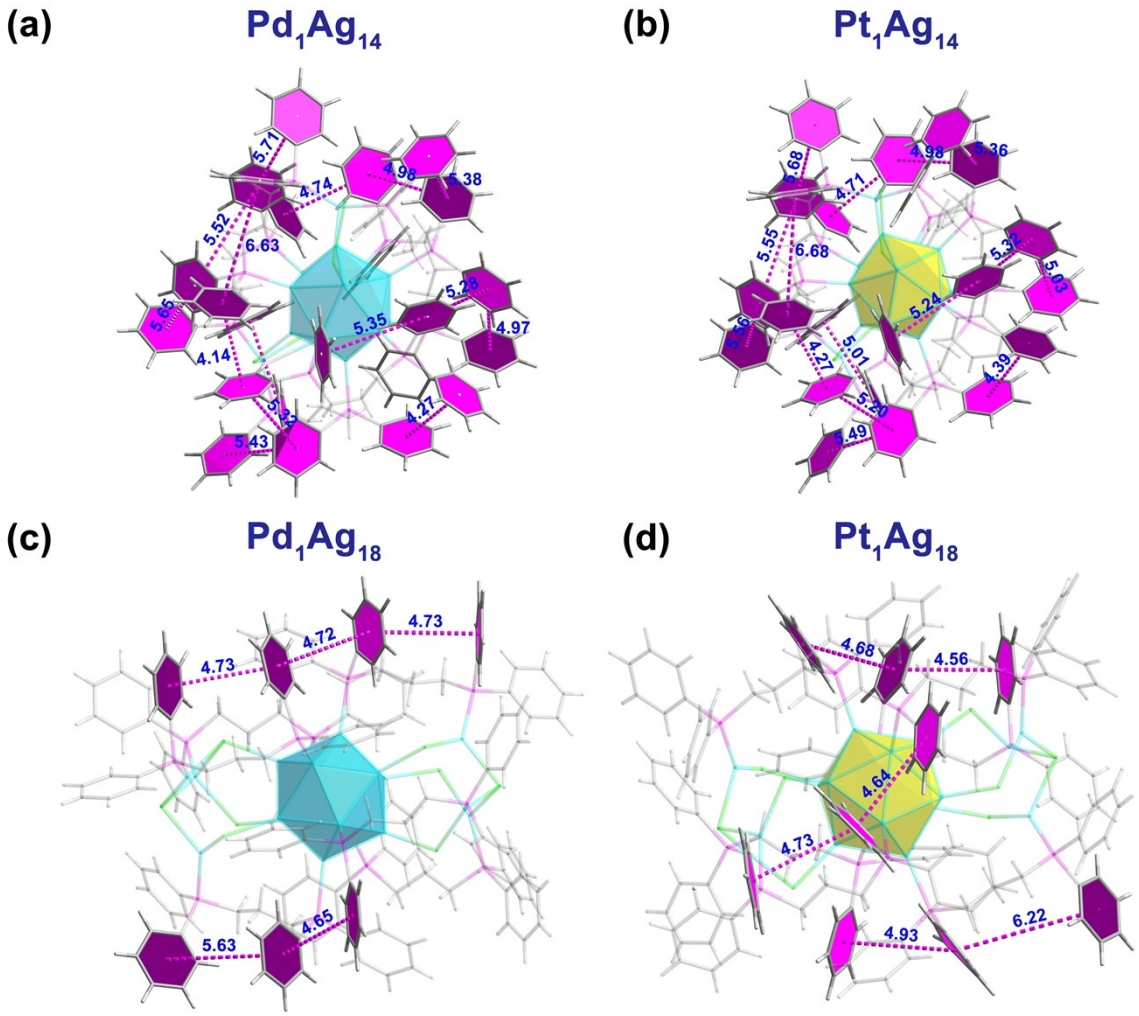

Fig. S39 Illustration of the intra-cluster non-covalent parallel-displaced π···π interactions and T-shape π···π interactions of M_1Ag_{14} (a, b) and M_1Ag_{18} (c, d) (M = Pd, Pt). The measured distances are indicated by dashed lines, and the blue numbers mark the distance between two planes in the intra-cluster parallel-displaced π···π interactions. Color code: dark green, Pd; yellow, Pt; sky blue, Ag; bright green, Cl; magenta, P; gray, C and white, H.

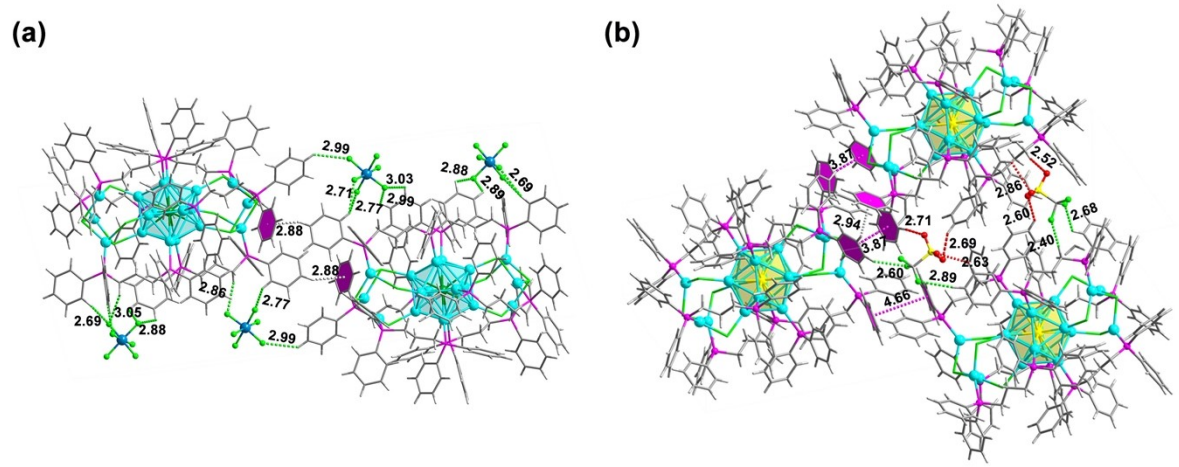

Fig. S40 Schematic illustration of the noncovalent interactions, including C–H···π, C–H···F/O, and π···π interactions, between clusters or between clusters and counterions in the Pd_1Ag_{18} (a) and Pt_1Ag_{18} (b) structures. The dashed lines correspond to the measured distances.

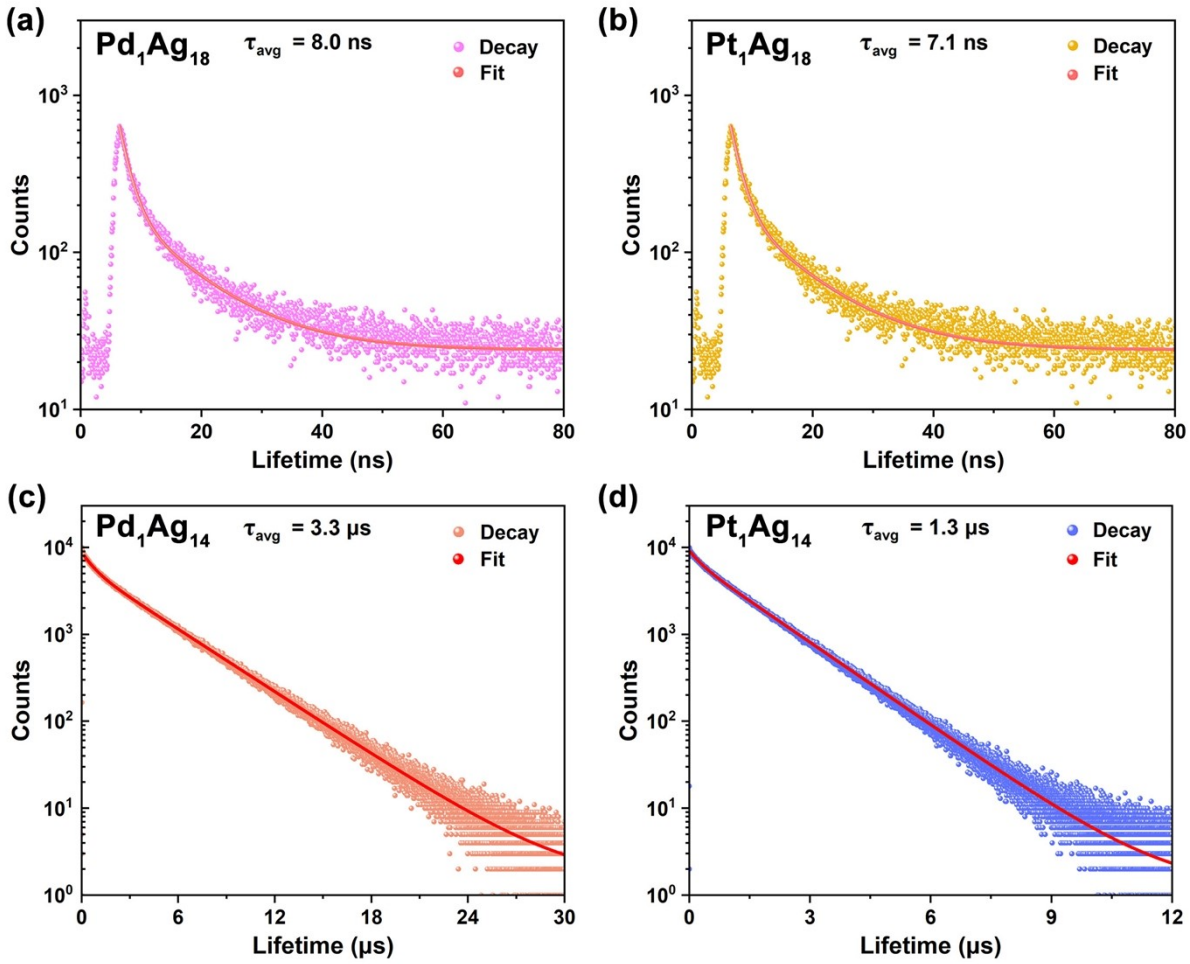

Fig. S41 PL decay profiles of M_1Ag_{18} (a, b) and M_1Ag_{14} (c, d). The data for M_1Ag_{14} are from our previous work[1].

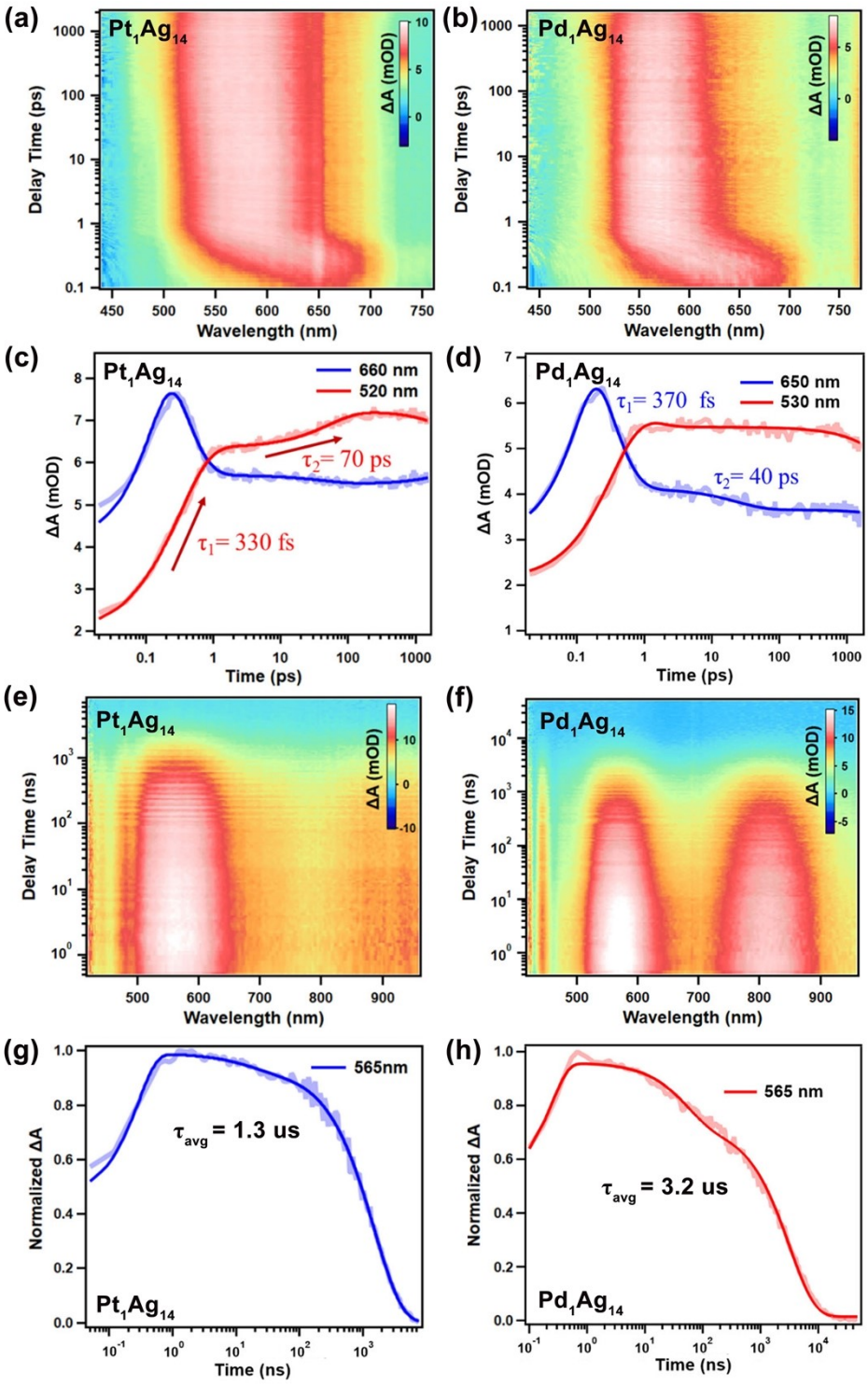

Fig. S42 Fs-TA data map of Pt_1Ag_{14} (a) and Pd_1Ag_{14} (b) in DMF with 360 nm excitation. FS-TA kinetic traces and corresponding fits of Pt_1Ag_{14} (c) and Pd_1Ag_{14} (d) at selected probe wavelengths. Ns-TA data map of Pt_1Ag_{14} (e) and Pd_1Ag_{14} (f) in DMF with 360 nm excitation. NS-TA kinetic traces and corresponding fits of Pt_1Ag_{14} (g) and Pd_1Ag_{14} (h) at selected probe wavelengths. The data for M_1Ag_{14} are from our previous work[1].

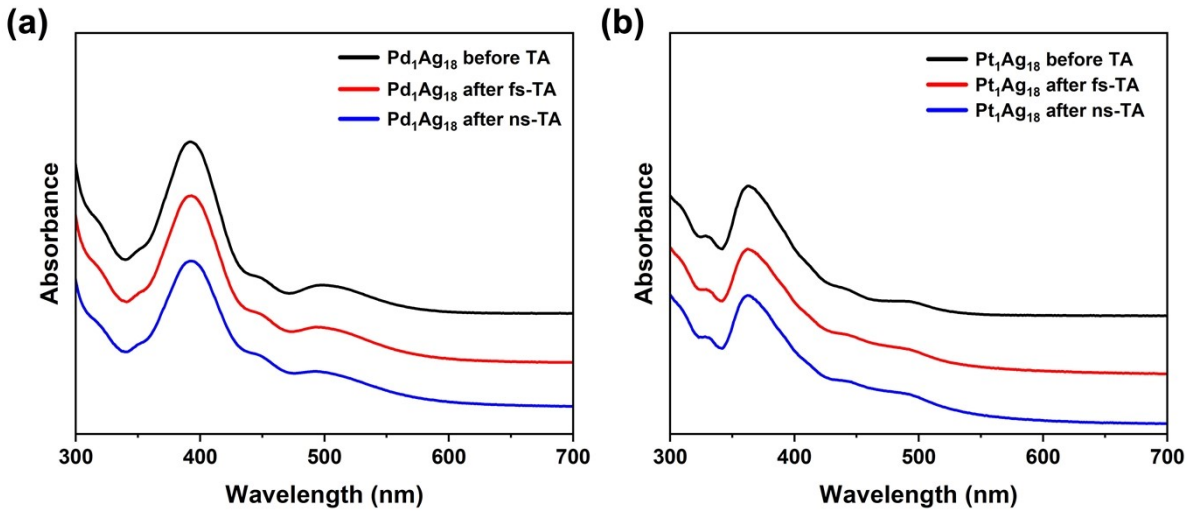

Fig. S43 UV-Vis spectra of (a) Pd_1Ag_{18} and (b) Pt_1Ag_{18} in DMF solution before and after fs/ns-TA experiments.

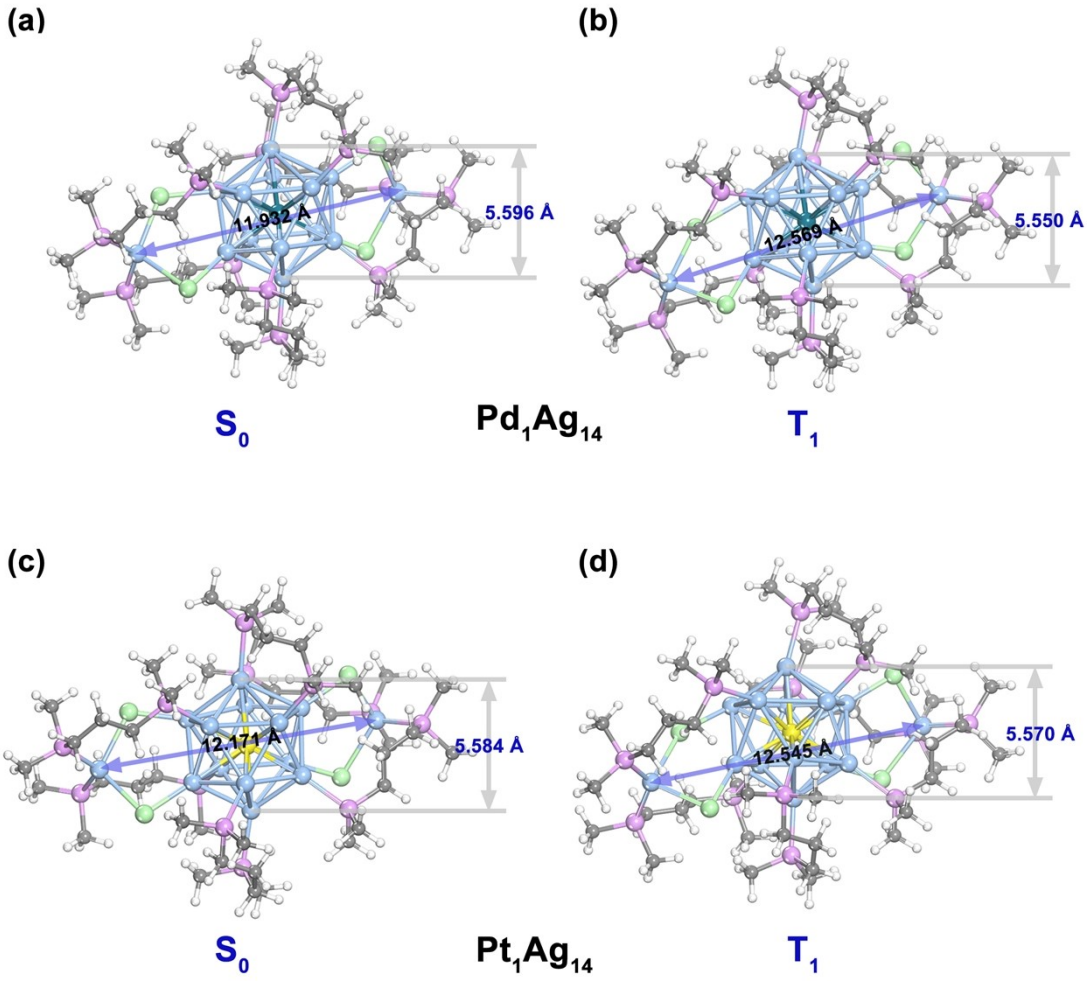

Fig. S44 Comparison between the optimized S_0 ground state (a,c) and T_1 excited state (b,d) structures of M_1Ag_{14}.

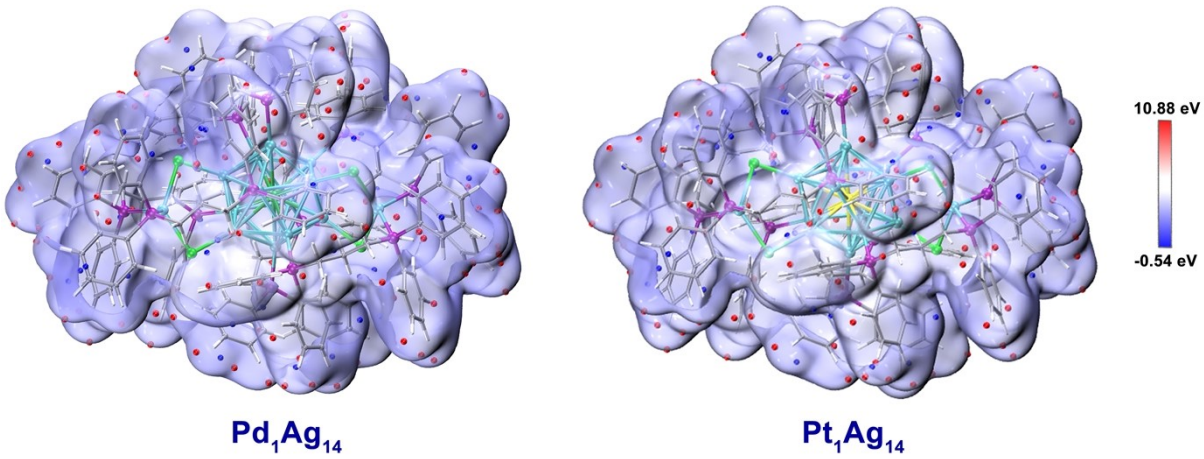

Fig. S45 Electrostatic potential (ESP) maps over the van der Waals surface (isovalue 0.001 a.u.) for M_1Ag_{14} clusters. Red and blue balls indicate local maxima and minima points of electrostatic potential isosurface, respectively.

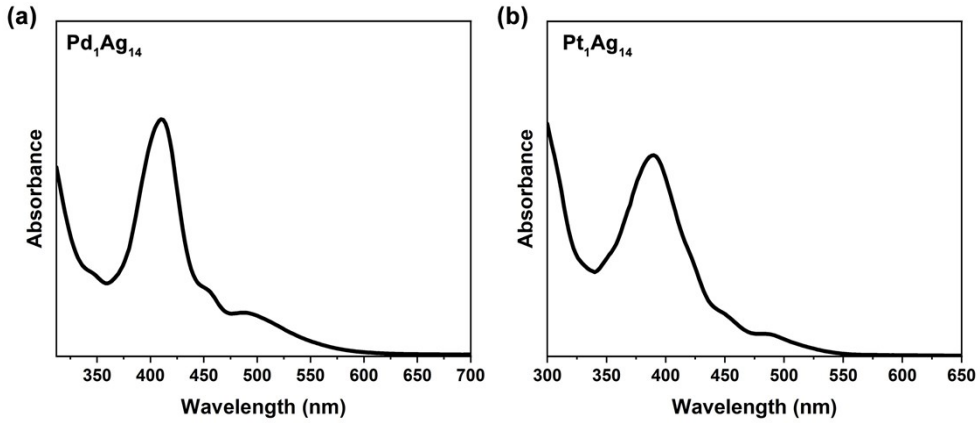

Fig. S46 UV-Vis spectra of M_1Ag_{14} crystals after 365 nm UV lamp (5W) irradiation for 2h and subsequent dissolution in DCM.

Table S1. Crystal data and structure refinement for the $[Pt_1Ag_{18}(DPPP)_6Cl_8][OTf]_2$ and $[Pd_1Ag_{18}(DPPP)_8Cl_8][SbF_6]_2$ nanoclusters with the CCDC number of 2476701 and 2476700.

Identification code	Pt_1Ag_{18}	Pd_1Ag_{18}
Formula	$C_{165}H_{158}Ag_{18}Cl_{10}F_6O_6P_{12}PtS_2$	$C_{162}H_{156}Ag_{18}Cl_8F_{12}P_{12}PdSb_2$
Fw	5277.91	5277.66
T (K)	193.00	193.00
Crystal system	triclinic	triclinic
Space group	P-1	P-1
a (Å)	16.6322(9)	16.658(2)
b (Å)	17.3464(9)	17.584(3)
c (Å)	37.675(2)	37.989(5)
α (°)	98.642(2)	89.479(7)
β (°)	93.062(2)	86.573(4)
γ (°)	117.567(2)	61.889(4)
V (Å^3)	9432.0(9)	9795(3)
Z	2	2
ρ_{calc} (g·cm^{-3})	1.858	1.789
μ (mm^{-1})	12.631	12.919
F (000)	5112.0	5092.0
Radiation	GaKα (λ = 1.34139)	GaKα (λ = 1.34139)
θ range for data collection (°)	4.168 to 108.3	4.958 to 109.098
Index ranges	-20 ≤ h ≤ 19, -20 ≤ k ≤ 20, -45 ≤ l ≤ 45	-20 ≤ h ≤ 20, -21 ≤ k ≤ 21, -45 ≤ l ≤45
Reflections collected	127307	105140
Independent reflections	34466	35886
R_{int}	0.0899	0.0909
R_{sigma}	0.0872	0.1050
Data/restraints/parameters	34466/3831/1885	35886/3721/1650
Goodness-of-fit on F^2	1.039	1.095
Final R indexes [I>=2σ (I)]	R_1 = 0.0808, wR_2 = 0.2067	R_1 = 0.1245, wR_2 = 0.2712
Final R indexes [all data]	R_1 = 0.1206, wR_2 = 0.2314	R_1 = 0.1737, wR_2 = 0.2988
Largest diff. peak and hole (e·Å^{-3})	3.81 and -2.48	2.28 and -2.22

Table S2. A summary of luminescent properties of M_1Ag_{14} and M_1Ag_{14} (M = Pd, Pt) superatoms dissolved in DMF.

Superatom	Φ^a (%)	τ_{avg}	k_r^b (s^{-1})	k_{nr}^c (s^{-1})
Pd_1Ag_{18}	**0.57**	**8.0 ns**	**7.13×10^5**	**1.24×10^8**
Pt_1Ag_{18}	**1.25**	**7.1 ns**	**1.76×10^6**	**1.39×10^8**
Pd_1Ag_{14}	**5.81**	**3.3 µs**	**1.76×10^4**	**2.85×10^5**
Pt_1Ag_{14}	**8.33**	**1.3µs**	**6.41×10^4**	**7.05×10^5**

Φ^a is the absolute quantum yield (QY). ^{b}Radiative decay rate constant: $k_r = \Phi/\tau_{avg}$. ^{c}Nonradiative decay rate constant: $k_{nr} = (1 - \Phi)/\tau_{avg}$.

Table S3. Composition of the superatomic 1S orbital of HOMO-278 in Pd_1Ag_{18} based on NAO method.

NAO#	Center	Label	Type	Composition
1	1(Pd)	s	Cor(4s)	1.904%
2	1(Pd)	s	Val(7s)	2.928%
50	2(Ag)	d_{yz}	Val(4d)	3.393%
52	2(Ag)	$d_{x^2-y^2}$	Val(4d)	1.195%
81	3(Ag)	d_{yz}	Val(4d)	3.610%
83	3(Ag)	$d_{x^2-y^2}$	Val(4d)	1.030%
106	4(Ag)	p_z	Val(5p)	0.659%
110	4(Ag)	d_{xz}	Val(4d)	0.539%
112	4(Ag)	d_{yz}	Val(4d)	1.036%
116	4(Ag)	d_{z^2}	Val(4d)	3.168%
134	5(Ag)	p_y	Val(5p)	0.561%

143	5(Ag)	d_{yz}	Val(4d)	1.530%
145	5(Ag)	$d_{x^2-y^2}$	Val(4d)	2.779%
147	5(Ag)	d_{z^2}	Val(4d)	0.520%
170	6(Ag)	d_{xy}	Val(4d)	1.313%
178	6(Ag)	d_{z^2}	Val(4d)	0.508%
199	7(Ag)	p_z	Val(5p)	0.599%
203	7(Ag)	d_{xz}	Val(4d)	0.506%
209	7(Ag)	d_{z^2}	Val(4d)	3.803%
227	8(Ag)	p_y	Val(5p)	0.585%
236	8(Ag)	d_{yz}	Val(4d)	0.929%
238	8(Ag)	$d_{x^2-y^2}$	Val(4d)	2.772%
240	8(Ag)	d_{z^2}	Val(4d)	0.666%
265	9(Ag)	d_{xz}	Val(4d)	1.580%
269	9(Ag)	$d_{x^2-y^2}$	Val(4d)	0.839%
286	10(Ag)	p_x	Val(5p)	0.627%
294	10(Ag)	d_{xy}	Val(4d)	0.726%
296	10(Ag)	d_{xz}	Val(4d)	0.534%
300	10(Ag)	$d_{x^2-y^2}$	Val(4d)	0.893%
317	11(Ag)	p_x	Val(5p)	0.527%
325	11(Ag)	d_{xy}	Val(4d)	0.598%
327	11(Ag)	d_{xz}	Val(4d)	0.635%
331	11(Ag)	$d_{x^2-y^2}$	Val(4d)	0.701%
348	12(Ag)	p_x	Val(5p)	0.539%
358	12(Ag)	d_{xz}	Val(4d)	1.644%
362	12(Ag)	$d_{x^2-y^2}$	Val(4d)	1.055%

379	13(Ag)	p_x	Val(5p)	0.510%
387	13(Ag)	d_{xy}	Val(4d)	1.277%
637	22(P)	p_z	Val(3p)	0.573%
652	23(P)	p_y	Val(3p)	0.567%
691	25(P)	p_z	Val(3p)	0.552%
739	28(Cl)	p_x	Val(3p)	0.656%
778	30(P)	p_y	Val(3p)	0.572%
829	33(Cl)	p_x	Val(3p)	0.523%

Note: All NAOs/shells whose contributions ≤ 0.50 % will not be listed.

Val: valence shell NAO; Cor: core NAO.

Table S4. Composition of the superatomic 1S orbital of HOMO-297 in Pt_1Ag_{18} based on NAO method.

NAO#	Center	Label	Type	Composition
1	1(Pt)	s	Cor(5s)	1.143%
2	1(Pt)	s	Val(7s)	2.602%
51	2(Ag)	d_{yz}	Val(4d)	1.252%
82	3(Ag)	d_{yz}	Val(4d)	0.755%
117	4(Ag)	d_z^2	Val(4d)	0.880%
146	5(Ag)	$d_{x^2-y^2}$	Val(4d)	0.634%
171	6(Ag)	d_{xy}	Val(4d)	0.564%
210	7(Ag)	d_z^2	Val(4d)	1.171%
239	8(Ag)	$d_{x^2-y^2}$	Val(4d)	0.624%
266	9(Ag)	d_{xz}	Val(4d)	0.659%

359	12(Ag)	d_{xz}	Val(4d)	0.621%
388	13(Ag)	d_{xy}	Val(4d)	0.531%
902	37(P)	p_x	Val(3p)	0.523%
938	39(P)	p_x	Val(3p)	0.974%
992	44(C)	p_x	Val(2p)	0.776%
1115	56(C)	p_x	Val(2p)	0.734%
1529	101(C)	p_x	Val(2p)	0.536%
1671	116(C)	p_z	Val(2p)	0.514%
1754	124(C)	p_y	Val(2p)	0.686%
2060	156(C)	p_z	Val(2p)	0.627%
2117	162(C)	p_z	Val(2p)	0.598%
2160	167(C)	p_z	Val(2p)	0.766%
2436	196(C)	p_x	Val(2p)	0.669%
2438	196(C)	p_y	Val(2p)	0.581%
2777	231(C)	p_z	Val(2p)	0.530%
2794	233(C)	p_y	Val(2p)	2.742%
2803	234(H)	s	Val(1s)	1.057%
2834	237(C)	p_z	Val(2p)	0.510%
2851	239(C)	p_y	Val(2p)	2.615%
2860	240(H)	s	Val(1s)	0.947%
2903	244(C)	p_y	Val(2p)	0.575%
2960	250(C)	p_y	Val(2p)	0.783%
2976	251(C)	p_z	Val(2p)	1.659%
2983	252(H)	s	Val(1s)	0.613%
3033	257(C)	p_z	Val(2p)	1.756%

3040	258(H)	s	Val(1s)	0.645%
3147	269(C)	p_z	Val(2p)	0.759%
3539	310(C)	p_y	Val(2p)	0.598%

Note: All NAOs/shells whose contributions ≤ 0.50 % will not be listed.

Val: valence shell NAO; Cor: core NAO.

Table S5. Composition of the superatomic $1P_x$ orbital (HOMO-2) in Pt_1Ag_{18} based on NAO method.

NAO#	Center	Label	Type	Composition
7	1(Pt)	p_x	Cor(5p)	0.699%
8	1(Pt)	p_x	Val(6p)	30.173%
39	2(Ag)	p_x	Val(5p)	1.284%
47	2(Ag)	d_{xy}	Val(4d)	0.616%
49	2(Ag)	d_{xz}	Val(4d)	0.516%
70	3(Ag)	p_x	Val(5p)	1.160%
78	3(Ag)	d_{xy}	Val(4d)	0.635%
101	4(Ag)	p_x	Val(5p)	1.385%
111	4(Ag)	d_{xz}	Val(4d)	0.982%
132	5(Ag)	p_x	Val(5p)	0.945%
140	5(Ag)	d_{xy}	Val(4d)	0.931%
157	6(Ag)	s	Cor(4s)	0.537%
158	6(Ag)	s	Val(5s)	1.186%
166	6(Ag)	p_y	Val(5p)	0.543%
177	6(Ag)	$d_{x^2-y^2}$	Val(4d)	0.994%

194	7(Ag)	p_x	Val(5p)	0.982%
204	7(Ag)	d_{xz}	Val(4d)	1.028%
225	8(Ag)	p_x	Val(5p)	1.126%
233	8(Ag)	d_{xy}	Val(4d)	0.870%
250	9(Ag)	s	Cor(4s)	0.602%
251	9(Ag)	s	Val(5s)	1.364%
262	9(Ag)	p_z	Val(5p)	0.524%
270	9(Ag)	$d_{x^2-y^2}$	Val(4d)	0.558%
281	10(Ag)	s	Cor(4s)	0.632%
282	10(Ag)	s	Val(5s)	1.143%
301	10(Ag)	$d_{x^2-y^2}$	Val(4d)	0.929%
312	11(Ag)	s	Cor(4s)	0.684%
313	11(Ag)	s	Val(5s)	1.595%
332	11(Ag)	$d_{x^2-y^2}$	Val(4d)	0.925%
343	12(Ag)	s	Cor(4s)	0.630%
344	12(Ag)	s	Val(5s)	1.339%
363	12(Ag)	$d_{x^2-y^2}$	Val(4d)	0.726%
365	12(Ag)	d_{z^2}	Val(4d)	0.566%
374	13(Ag)	s	Cor(4s)	0.517%
375	13(Ag)	s	Val(5s)	0.964%
394	13(Ag)	$d_{x^2-y^2}$	Val(4d)	1.687%
668	24(Cl)	p_x	Val(3p)	1.921%
671	24(Cl)	p_y	Val(3p)	0.796%
674	24(Cl)	p_z	Val(3p)	1.057%
704	26(Cl)	p_x	Val(3p)	1.435%

707	26(Cl)	p_y	Val(3p)	1.949%
740	28(Cl)	p_x	Val(3p)	2.039%
746	28(Cl)	p_z	Val(3p)	1.272%
794	31(Cl)	p_x	Val(3p)	2.329%
797	31(Cl)	p_y	Val(3p)	1.341%
830	33(Cl)	p_x	Val(3p)	3.140%
833	33(Cl)	p_y	Val(3p)	0.841%
866	35(Cl)	p_x	Val(3p)	1.318%
872	35(Cl)	p_z	Val(3p)	1.913%

Note: All NAOs/shells whose contributions ≤ 0.50 % will not be listed.

Val: valence shell NAO; Cor: core NAO.

Table S6. Composition of the superatomic $1P_z$ orbital (HOMO-1) in Pt_1Ag_{18} based on NAO method.

NAO#	**Center**	**Label**	**Type**	**Composition**
11	1(Pt)	p_y	Val(6p)	2.534%
13	1(Pt)	p_z	Cor(5p)	0.605%
14	1(Pt)	p_z	Val(6p)	24.315%
34	2(Ag)	s	Val(5s)	1.111%
42	2(Ag)	p_y	Val(5p)	1.162%
51	2(Ag)	d_{yz}	Val(4d)	0.757%
65	3(Ag)	s	Val(5s)	0.852%
73	3(Ag)	p_y	Val(5p)	1.145%

82	3(Ag)	d_{yz}	Val(4d)	0.699%
86	3(Ag)	d_z^2	Val(4d)	0.630%
96	4(Ag)	s	Val(5s)	1.132%
107	4(Ag)	p_z	Val(5p)	0.590%
117	4(Ag)	d_z^2	Val(4d)	0.882%
138	5(Ag)	p_z	Val(5p)	0.839%
144	5(Ag)	d_{yz}	Val(4d)	0.570%
173	6(Ag)	d_{xz}	Val(4d)	0.922%
175	6(Ag)	d_{yz}	Val(4d)	0.605%
189	7(Ag)	s	Val(5s)	0.910%
200	7(Ag)	p_z	Val(5p)	0.755%
210	7(Ag)	d_z^2	Val(4d)	1.121%
231	8(Ag)	p_z	Val(5p)	0.764%
237	8(Ag)	d_{yz}	Val(4d)	0.706%
251	9(Ag)	s	Val(5s)	0.637%
272	9(Ag)	d_z^2	Val(4d)	0.736%
282	10(Ag)	s	Val(5s)	0.711%
328	11(Ag)	d_{xz}	Val(4d)	0.651%
344	12(Ag)	s	Val(5s)	0.797%
365	12(Ag)	d_z^2	Val(4d)	0.575%
386	13(Ag)	p_z	Val(5p)	0.526%
390	13(Ag)	d_{xz}	Val(4d)	0.970%
593	20(P)	s	Val(3s)	1.223%
599	20(P)	p_y	Val(3p)	2.716%
602	20(P)	p_z	Val(3p)	1.963%

611	21(P)	s	Val(3s)	1.119%
617	21(P)	p_y	Val(3p)	0.624%
620	21(P)	p_z	Val(3p)	3.610%
629	22(P)	s	Val(3s)	1.302%
635	22(P)	p_y	Val(3p)	1.921%
638	22(P)	p_z	Val(3p)	2.962%
668	24(Cl)	p_x	Val(3p)	1.109%
683	25(P)	s	Val(3s)	1.257%
692	25(P)	p_z	Val(3p)	4.326%
740	28(Cl)	p_x	Val(3p)	0.835%
866	35(Cl)	p_x	Val(3p)	0.712%

Note: All NAOs/shells whose contributions ≤ 0.50 % will not be listed.

Val: valence shell NAO; Cor: core NAO.

Table S7. Composition of the superatomic $1P_y$ orbital (HOMO) in Pt_1Ag_{18} based on NAO method.

NAO#	**Center**	**Label**	**Type**	**Composition**
10	1(Pt)	p_y	Cor(5p)	0.604%
11	1(Pt)	p_y	Val(6p)	24.404%
14	1(Pt)	p_z	Val(6p)	2.544%
45	2(Ag)	p_z	Val(5p)	1.002%
53	2(Ag)	$d_{x^2-y^2}$	Val(4d)	0.543%
55	2(Ag)	d_{z^2}	Val(4d)	0.514%
76	3(Ag)	p_z	Val(5p)	0.990%

107	4(Ag)	p_z	Val(5p)	0.702%
113	4(Ag)	d_{yz}	Val(4d)	1.332%
126	5(Ag)	s	Cor(4s)	0.601%
127	5(Ag)	s	Val(5s)	1.254%
135	5(Ag)	p_y	Val(5p)	0.980%
146	5(Ag)	$d_{x^2-y^2}$	Val(4d)	0.709%
158	6(Ag)	s	Val(5s)	0.941%
177	6(Ag)	$d_{x^2-y^2}$	Val(4d)	0.687%
189	7(Ag)	s	Val(5s)	0.537%
206	7(Ag)	d_{yz}	Val(4d)	0.687%
219	8(Ag)	s	Cor(4s)	0.601%
220	8(Ag)	s	Val(5s)	1.290%
228	8(Ag)	p_y	Val(5p)	1.075%
239	8(Ag)	$d_{x^2-y^2}$	Val(4d)	0.998%
264	9(Ag)	d_{xy}	Val(4d)	0.893%
268	9(Ag)	d_{yz}	Val(4d)	0.723%
295	10(Ag)	d_{xy}	Val(4d)	0.790%
326	11(Ag)	d_{xy}	Val(4d)	0.516%
357	12(Ag)	d_{xy}	Val(4d)	0.691%
361	12(Ag)	d_{yz}	Val(4d)	0.562%
375	13(Ag)	s	Val(5s)	1.149%
380	13(Ag)	p_x	Val(5p)	0.545%
599	20(P)	p_y	Val(3p)	1.201%
611	21(P)	s	Val(3s)	0.539%
620	21(P)	p_z	Val(3p)	1.518%

635	22(P)	p_y	Val(3p)	0.769%
638	22(P)	p_z	Val(3p)	0.714%
647	23(P)	s	Val(3s)	1.585%
653	23(P)	p_y	Val(3p)	5.018%
656	23(P)	p_z	Val(3p)	0.684%
692	25(P)	p_z	Val(3p)	1.241%
704	26(Cl)	p_x	Val(3p)	1.239%
773	30(P)	s	Val(3s)	1.638%
779	30(P)	p_y	Val(3p)	5.760%
794	31(Cl)	p_x	Val(3p)	1.018%
866	35(Cl)	p_x	Val(3p)	0.508%

Note: All NAOs/shells whose contributions ≤ 0.50 % will not be listed.

Val: valence shell NAO; Cor: core NAO.

Table S8. Composition of the superatomic $1D_Z^2$ orbital (LUMO) in Pt_1Ag_{18} based on NAO method.

NAO#	**Center**	**Label**	**Type**	**Composition**
16	1(Pt)	d_{xy}	Val(5d)	1.963%
18	1(Pt)	d_{xz}	Val(5d)	1.371%
24	1(Pt)	d_z^2	Val(5d)	1.223%
42	2(Ag)	p_y	Val(5p)	1.968%
45	2(Ag)	p_z	Val(5p)	2.295%
73	3(Ag)	p_y	Val(5p)	1.573%
76	3(Ag)	p_z	Val(5p)	1.940%

101	4(Ag)	p_x	Val(5p)	5.522%
104	4(Ag)	p_y	Val(5p)	2.566%
107	4(Ag)	p_z	Val(5p)	0.608%
132	5(Ag)	p_x	Val(5p)	5.641%
158	6(Ag)	s	Val(5s)	3.838%
169	6(Ag)	p_z	Val(5p)	1.392%
171	6(Ag)	d_{xy}	Val(4d)	0.726%
194	7(Ag)	p_x	Val(5p)	3.098%
197	7(Ag)	p_y	Val(5p)	1.644%
225	8(Ag)	p_x	Val(5p)	6.160%
251	9(Ag)	s	Val(5s)	2.484%
321	11(Ag)	p_y	Val(5p)	1.353%
344	12(Ag)	s	Val(5s)	2.525%
352	12(Ag)	p_y	Val(5p)	0.908%
355	12(Ag)	p_z	Val(5p)	0.615%
375	13(Ag)	s	Val(5s)	4.244%
383	13(Ag)	p_y	Val(5p)	0.663%
388	13(Ag)	d_{xy}	Val(4d)	0.536%
704	26(Cl)	p_x	Val(3p)	1.059%
740	28(Cl)	p_x	Val(3p)	0.759%
791	31(Cl)	s	Val(3s)	0.503%
794	31(Cl)	p_x	Val(3p)	1.479%
866	35(Cl)	p_x	Val(3p)	0.861%

Note: All NAOs/shells whose contributions ≤ 0.50 % will not be listed.

Val: valence shell NAO; Cor: core NAO.

Table S9. Composition of the superatomic $1P_x$ orbital (HOMO-2) in Pd_1Ag_{18} based on NAO method.

NAO#	Center	Label	Type	Composition
6	1(Pd)	p_x	Cor(4p)	0.561%
7	1(Pd)	p_x	Val(5p)	27.942%
38	2(Ag)	p_x	Val(5p)	1.243%
46	2(Ag)	d_{xy}	Val(4d)	0.548%
69	3(Ag)	p_x	Val(5p)	1.143%
77	3(Ag)	d_{xy}	Val(4d)	0.579%
100	4(Ag)	p_x	Val(5p)	1.388%
110	4(Ag)	d_{xz}	Val(4d)	0.910%
131	5(Ag)	p_x	Val(5p)	0.874%
139	5(Ag)	d_{xy}	Val(4d)	0.835%
157	6(Ag)	s	Val(5s)	1.293%
165	6(Ag)	p_y	Val(5p)	0.733%
176	6(Ag)	$d_{x^2-y^2}$	Val(4d)	0.976%
193	7(Ag)	p_x	Val(5p)	0.924%
203	7(Ag)	d_{xz}	Val(4d)	0.922%
224	8(Ag)	p_x	Val(5p)	1.103%
232	8(Ag)	d_{xy}	Val(4d)	0.805%
249	9(Ag)	s	Cor(4s)	0.564%
250	9(Ag)	s	Val(5s)	1.518%
261	9(Ag)	p_z	Val(5p)	0.728%
269	9(Ag)	$d_{x^2-y^2}$	Val(4d)	0.562%

280	10(Ag)	s	Cor(4s)	0.585%
281	10(Ag)	s	Val(5s)	1.268%
300	10(Ag)	$d_{x^2-y^2}$	Val(4d)	0.904%
302	10(Ag)	d_{z^2}	Val(4d)	0.501%
311	11(Ag)	s	Cor(4s)	0.648%
312	11(Ag)	s	Val(5s)	1.772%
331	11(Ag)	$d_{x^2-y^2}$	Val(4d)	0.925%
342	12(Ag)	s	Cor(4s)	0.593%
343	12(Ag)	s	Val(5s)	1.476%
354	12(Ag)	p_z	Val(5p)	0.531%
362	12(Ag)	$d_{x^2-y^2}$	Val(4d)	0.741%
374	13(Ag)	s	Val(5s)	1.075%
382	13(Ag)	p_y	Val(5p)	0.561%
393	13(Ag)	$d_{x^2-y^2}$	Val(4d)	1.575%
667	24(Cl)	p_x	Val(3p)	1.999%
670	24(Cl)	p_y	Val(3p)	0.808%
673	24(Cl)	p_z	Val(3p)	1.105%
703	26(Cl)	p_x	Val(3p)	1.454%
706	26(Cl)	p_y	Val(3p)	1.994%
739	28(Cl)	p_x	Val(3p)	2.161%
745	28(Cl)	p_z	Val(3p)	1.284%
793	31(Cl)	p_x	Val(3p)	2.384%
796	31(Cl)	p_y	Val(3p)	1.320%
829	33(Cl)	p_x	Val(3p)	3.258%
832	33(Cl)	p_y	Val(3p)	0.835%

865	35(Cl)	p_x	Val(3p)	1.383%
871	35(Cl)	p_z	Val(3p)	1.971%

Note: All NAOs/shells whose contributions ≤ 0.50 % will not be listed.

Val: valence shell NAO; Cor: core NAO.

Table S10. Composition of the superatomic $1P_z$ orbital (HOMO-1) in Pd_1Ag_{18} based on NAO method.

NAO#	Center	Label	Type	Composition
10	1(Pd)	p_y	Val(5p)	2.566%
13	1(Pd)	p_z	Val(5p)	21.271%
33	2(Ag)	s	Val(5s)	1.395%
41	2(Ag)	p_y	Val(5p)	1.550%
50	2(Ag)	d_{yz}	Val(4d)	0.805%
64	3(Ag)	s	Val(5s)	1.103%
72	3(Ag)	p_y	Val(5p)	1.452%
81	3(Ag)	d_{yz}	Val(4d)	0.750%
85	3(Ag)	d_z^2	Val(4d)	0.590%
95	4(Ag)	s	Val(5s)	1.341%
103	4(Ag)	p_y	Val(5p)	0.575%
106	4(Ag)	p_z	Val(5p)	0.837%
116	4(Ag)	d_z^2	Val(4d)	0.887%
137	5(Ag)	p_z	Val(5p)	0.869%
143	5(Ag)	dyz	Val(4d)	0.501%
172	6(Ag)	d_{xz}	Val(4d)	0.843%

174	6(Ag)	d_{yz}	Val(4d)	0.548%
188	7(Ag)	s	Val(5s)	1.073%
196	7(Ag)	p_y	Val(5p)	0.511%
199	7(Ag)	p_z	Val(5p)	1.117%
209	7(Ag)	d_z^2	Val(4d)	1.143%
230	8(Ag)	p_z	Val(5p)	0.773%
236	8(Ag)	d_{yz}	Val(4d)	0.626%
250	9(Ag)	s	Val(5s)	0.648%
271	9(Ag)	d_z^2	Val(4d)	0.663%
281	10(Ag)	s	Val(5s)	0.750%
327	11(Ag)	d_{xz}	Val(4d)	0.635%
343	12(Ag)	s	Val(5s)	0.832%
348	12(Ag)	p_x	Val(5p)	0.616%
364	12(Ag)	d_z^2	Val(4d)	0.518%
385	13(Ag)	p_z	Val(5p)	0.531%
389	13(Ag)	d_{xz}	Val(4d)	0.884%
592	20(P)	s	Val(3s)	1.311%
598	20(P)	p_y	Val(3p)	2.853%
601	20(P)	p_z	Val(3p)	2.100%
610	21(P)	s	Val(3s)	1.124%
616	21(P)	p_y	Val(3p)	0.618%
619	21(P)	p_z	Val(3p)	3.576%
628	22(P)	s	Val(3s)	1.388%
634	22(P)	p_y	Val(3p)	2.056%
637	22(P)	p_z	Val(3p)	3.094%

667	24(Cl)	p_x	Val(3p)	1.164%
682	25(P)	s	Val(3s)	1.266%
691	25(P)	p_z	Val(3p)	4.310%
739	28(Cl)	p_x	Val(3p)	0.904%
865	35(Cl)	p_x	Val(3p)	0.719%

Note: All NAOs/shells whose contributions ≤ 0.50 % will not be listed.

Val: valence shell NAO; Cor: core NAO.

Table S11. Composition of the superatomic $1P_y$ orbital (HOMO) in Pd_1Ag_{18} based on NAO method.

NAO#	Center	Label	Type	Composition
10	1(Pd)	p_y	Val(5p)	21.363%
13	1(Pd)	p_z	Val(5p)	2.582%
44	2(Ag)	p_z	Val(5p)	1.136%
52	2(Ag)	$d_{x^2-y^2}$	Val(4d)	0.507%
64	3(Ag)	s	Val(5s)	0.566%
75	3(Ag)	p_z	Val(5p)	1.132%
106	4(Ag)	p_z	Val(5p)	0.972%
112	4(Ag)	d_{yz}	Val(4d)	1.268%
125	5(Ag)	s	Cor(4s)	0.561%
126	5(Ag)	s	Val(5s)	1.523%
134	5(Ag)	p_y	Val(5p)	1.464%
145	5(Ag)	$d_{x^2-y^2}$	Val(4d)	0.736%
157	6(Ag)	s	Val(5s)	1.004%

162	6(Ag)	p_x	Val(5p)	0.659%
176	6(Ag)	$d_{x^2-y^2}$	Val(4d)	0.587%
188	7(Ag)	s	Val(5s)	0.681%
199	7(Ag)	p_z	Val(5p)	0.714%
205	7(Ag)	d_{yz}	Val(4d)	0.635%
218	8(Ag)	s	Cor(4s)	0.562%
219	8(Ag)	s	Val(5s)	1.585%
227	8(Ag)	p_y	Val(5p)	1.610%
238	8(Ag)	$d_{x^2-y^2}$	Val(4d)	1.022%
263	9(Ag)	d_{xy}	Val(4d)	0.828%
267	9(Ag)	d_{yz}	Val(4d)	0.658%
294	10(Ag)	d_{xy}	Val(4d)	0.757%
356	12(Ag)	d_{xy}	Val(4d)	0.612%
360	12(Ag)	d_{yz}	Val(4d)	0.508%
374	13(Ag)	s	Val(5s)	1.208%
379	13(Ag)	p_x	Val(5p)	0.750%
598	20(P)	p_y	Val(3p)	1.100%
610	21(P)	s	Val(3s)	0.602%
616	21(P)	p_y	Val(3p)	0.518%
619	21(P)	p_z	Val(3p)	1.690%
634	22(P)	p_y	Val(3p)	0.719%
637	22(P)	p_z	Val(3p)	0.676%
646	23(P)	s	Val(3s)	1.641%
652	23(P)	p_y	Val(3p)	5.162%
655	23(P)	p_z	Val(3p)	0.677%

691	25(P)	p_z	Val(3p)	1.421%
703	26(Cl)	p_x	Val(3p)	1.284%
772	30(P)	s	Val(3s)	1.700%
778	30(P)	p_y	Val(3p)	5.890%
793	31(Cl)	p_x	Val(3p)	1.132%
865	35(Cl)	p_x	Val(3p)	0.555%

Note: All NAOs/shells whose contributions ≤ 0.50 % will not be listed.

Val: valence shell NAO; Cor: core NAO.

Table S12. Composition of the superatomic $1D_z^2$ orbital (LUMO) in Pd_1Ag_{18} based on NAO method.

NAO#	Center	Label	Type	Composition
15	1(Pd)	d_{xy}	Val(4d)	1.695%
17	1(Pd)	d_{xz}	Val(4d)	1.513%
23	1(Pd)	d_z^2	Val(4d)	1.179%
41	2(Ag)	p_y	Val(5p)	1.949%
44	2(Ag)	p_z	Val(5p)	2.372%
72	3(Ag)	p_y	Val(5p)	1.729%
75	3(Ag)	p_z	Val(5p)	1.952%
100	4(Ag)	p_x	Val(5p)	6.032%
103	4(Ag)	p_y	Val(5p)	2.173%
106	4(Ag)	p_z	Val(5p)	0.651%
131	5(Ag)	p_x	Val(5p)	5.645%
137	5(Ag)	p_z	Val(5p)	0.507%

157	6(Ag)	s	Val(5s)	3.889%
168	6(Ag)	p_z	Val(5p)	1.464%
170	6(Ag)	d_{xy}	Val(4d)	0.653%
193	7(Ag)	p_x	Val(5p)	3.806%
196	7(Ag)	p_y	Val(5p)	1.390%
224	8(Ag)	p_x	Val(5p)	6.017%
250	9(Ag)	s	Val(5s)	3.003%
265	9(Ag)	d_{xz}	Val(4d)	0.518%
292	10(Ag)	p_z	Val(5p)	0.564%
320	11(Ag)	p_y	Val(5p)	1.275%
343	12(Ag)	s	Val(5s)	3.010%
351	12(Ag)	p_y	Val(5p)	0.916%
354	12(Ag)	p_z	Val(5p)	0.699%
374	13(Ag)	s	Val(5s)	4.360%
382	13(Ag)	p_y	Val(5p)	0.587%
703	26(Cl)	p_x	Val(3p)	1.061%
739	28(Cl)	p_x	Val(3p)	0.887%
793	31(Cl)	p_x	Val(3p)	1.520%
865	35(Cl)	p_x	Val(3p)	1.065%

Note: All NAOs/shells whose contributions ≤ 0.50 % will not be listed.

Val: valence shell NAO; Cor: core NAO; Ryd: Rydberg NAO.

Table S13. Frontier orbital (HOMO-2 to LUMO) compositions for Pt_1Ag_{18} were determined using the NAO method, with the dominant contributions identified as originating from the Pt_1Ag_{12} core.

HOMO-2		HOMO-1		HOMO		LUMO	
Atom	**Composition**	**Atom**	**Composition**	**Atom**	**Composition**	**Atom**	**Composition**
1(Pt)	**31.110%**	**1(Pt)**	**27.668 %**	**1(Pt)**	**27.801%**	**1(Pt)**	**6.163%**
2(Ag)	**2.726%**	**2(Ag)**	**4.101 %**	**2(Ag)**	**2.679%**	**2(Ag)**	**4.970%**
3(Ag)	**2.527%**	**3(Ag)**	**4.256 %**	**3(Ag)**	**2.601%**	**3(Ag)**	**3.739%**
4(Ag)	**2.909%**	**4(Ag)**	**3.940 %**	**4(Ag)**	**3.009%**	**4(Ag)**	**8.927%**
5(Ag)	**2.640%**	**5(Ag)**	**1.952 %**	**5(Ag)**	**4.660%**	**5(Ag)**	**6.748%**
6(Ag)	**3.949%**	**6(Ag)**	**2.430 %**	**6(Ag)**	**2.900%**	**6(Ag)**	**7.994%**
7(Ag)	**2.525%**	**7(Ag)**	**4.155 %**	**7(Ag)**	**2.561%**	**7(Ag)**	**5.280%**
8(Ag)	**2.718%**	**8(Ag)**	**1.849 %**	**8(Ag)**	**4.961%**	**8(Ag)**	**6.820%**
9(Ag)	**3.941%**	**9(Ag)**	**2.607 %**	**9(Ag)**	**2.592%**	**9(Ag)**	**4.624%**
10(Ag)	**4.152%**	**10(Ag)**	**2.694 %**	**10(Ag)**	**2.707%**	**10(Ag)**	**1.183%**
11(Ag)	**4.231%**	**11(Ag)**	**2.761 %**	**11(Ag)**	**2.277%**	**11(Ag)**	**2.130%**
12(Ag)	**4.010%**	**12(Ag)**	**2.973 %**	**12(Ag)**	**2.272%**	**12(Ag)**	**5.889%**
13(Ag)	**4.093%**	**13(Ag)**	**2.436 %**	**13(Ag)**	**2.982%**	**13(Ag)**	**7.661%**
23(P)	0.573%	20(P)	6.004 %	20(P)	2.198%	21(P)	0.736%
24(Cl)	3.890%	21(P)	5.476 %	21(P)	2.630%	22(P)	0.510%
26(Cl)	3.482%	22(P)	6.274 %	22(P)	1.908%	23(P)	0.595%
28(Cl)	3.402%	24(Cl)	1.253 %	23(P)	7.458%	25(P)	0.605%
31(Cl)	3.932%	25(P)	5.823 %	25(P)	1.729%	26(Cl)	2.010%
33(Cl)	4.411%	26(Cl)	0.547 %	26(Cl)	1.427%	28(Cl)	1.133%
35(Cl)	3.415%	28(Cl)	0.970 %	30(P)	7.769%	30(P)	0.736%
		31(Cl)	0.527 %	31(Cl)	1.093%	31(Cl)	2.118%
		33(Cl)	0.529 %	33(Cl)	0.783%	35(Cl)	1.710%
		35(Cl)	0.860 %	35(Cl)	0.828%	79(C)	0.520%

						86(C)	0.683%
Note: All atoms whose contributions ≤ 0.50 % will not be listed.							

Table S14. Frontier orbital (HOMO-2 to LUMO) compositions for Pd_1Ag_{18} were determined using the NAO method, with the dominant contributions identified as originating from the Pd_1Ag_{12} core.

HOMO-2		**HOMO-1**		**HOMO**		**LUMO**	
Center	**Composition**	**Center**	**Composition**	**Center**	**Composition**	**Center**	**Composition**
1(Pd)	**28.699%**	**1(Pd)**	**24.493%**	**1(Pd)**	**24.649%**	**1(Pd)**	**5.631%**
2(Ag)	**2.605%**	**2(Ag)**	**4.896%**	**2(Ag)**	**2.715%**	**2(Ag)**	**4.768%**
3(Ag)	**2.405%**	**3(Ag)**	**4.970%**	**3(Ag)**	**2.722%**	**3(Ag)**	**3.867%**
4(Ag)	**2.849%**	**4(Ag)**	**4.495%**	**4(Ag)**	**3.235%**	**4(Ag)**	**9.089%**
5(Ag)	**2.565%**	**5(Ag)**	**1.886%**	**5(Ag)**	**5.499%**	**5(Ag)**	**6.955%**
6(Ag)	**4.257%**	**6(Ag)**	**2.281%**	**6(Ag)**	**2.997%**	**6(Ag)**	**8.103%**
7(Ag)	**2.395%**	**7(Ag)**	**4.674%**	**7(Ag)**	**2.862%**	**7(Ag)**	**5.751%**
8(Ag)	**2.678%**	**8(Ag)**	**1.745%**	**8(Ag)**	**5.820%**	**8(Ag)**	**6.853%**
9(Ag)	**4.357%**	**9(Ag)**	**2.563%**	**9(Ag)**	**2.540%**	**9(Ag)**	**5.561%**
10(Ag)	**4.522%**	**10(Ag)**	**2.691%**	**10(Ag)**	**2.606%**	**10(Ag)**	**1.280%**
11(Ag)	**4.697%**	**11(Ag)**	**2.795%**	**11(Ag)**	**2.122%**	**11(Ag)**	**2.018%**
12(Ag)	**4.367%**	**12(Ag)**	**3.087%**	**12(Ag)**	**2.144%**	**12(Ag)**	**6.646%**
13(Ag)	**4.335%**	**13(Ag)**	**2.278%**	**13(Ag)**	**3.150%**	**13(Ag)**	**7.801%**
23(P)	0.610%	20(P)	6.408%	20(P)	2.055%	21(P)	0.634%
24(Cl)	4.051%	21(P)	5.470%	21(P)	2.912%	23(P)	0.571%
26(Cl)	3.562%	22(P)	6.670%	22(P)	1.808%	25(P)	0.619%
28(Cl)	3.554%	24(Cl)	1.312%	23(P)	7.706%	26(Cl)	1.970%

31(Cl)	3.985%	25(P)	5.857%	25(P)	1.986%	28(Cl)	1.303%
33(Cl)	4.537%	26(Cl)	0.572%	26(Cl)	1.510%	30(P)	0.728%
35(Cl)	3.563%	28(Cl)	1.055%	30(P)	8.028%	31(Cl)	2.148%
		33(Cl)	0.590%	31(Cl)	1.227%	35(Cl)	2.004%
		35(Cl)	0.884%	33(Cl)	0.770%	86(C)	0.640%
				35(Cl)	0.869%		
Note: All atoms whose contributions ≤ 0.50 % will not be listed.							

Table S15. Continuous symmetry measure (CSM) values for the M@Ag_{12} cores of M_1Ag_{14} and M_1Ag_{18}.

Superatoms	Pd_1Ag_{14}	Pd_1Ag_{18}	Pt_1Ag_{14}	Pt_1Ag_{18}
CSM	0.0322	0.0227	0.0349	0.0322

References

1. B. Yin, J. Kong, M. Guo, J. Kong, Q. You, M. Zhou and Z. Luo, Heterometal Doping Modulates Luminescent and Chiroptical Behavior in Superatomic M_1Ag_{14} (M = Pd, Pt) Clusters, *Small*, 2025, **21**, 2504958.